Screening the Geomechanical Stability (Thermal & Mechanical) of Shared Multi-user CO2 Storage Assets, a Simple Effective Tool Applied to the Captain Sandstone Aquifer

Screening the Geomechanical Stability (Thermal & Mechanical) of Shared Multi-user CO2 Storage Assets, a Simple Effective Tool Applied to the Captain Sandstone Aquifer

*Christopher McDermott[1], John Williams[2], Owain Tucker[3], Min Jin[4], Eric Mackay[4], Katriona Edlmann[1], R. Stuart Haszeldine[1], Wenqing Wang[6], Olaf Kolditz[6], Maxine Akhurst[5]

*Corresponding author christopher.mcdermott@ed.ac.uk

[1]University of Edinburgh, School of Geosciences, Edinburgh, UK

[2]British Geological Survey, Keyworth, Nottingham, UK

[3]Shell Projects & Technology, Aberdeen, UK.

[4]Heriot-Watt University, Institute of Petroleum Engineering, Edinburgh, UK

[5]British Geological Survey, Edinburgh, UK.

[6]Helmholtz Center for Environmental Research, Leipzig, Germany.

Abstract

Multi-user stores are anticipated in the near future to permanently store CO_2 captured at industrial sources to meet emissions reductions targets. Multiple storage permit applications will be required to exploit the immense potential capacity within extensive CO_2 storage assets. To retain 99% of the injected CO_2 for 1000 years the geomechanical stability of the sealing strata above the pressurised storage reservoir is a key factor which needs to be included in the geo-engineering design of shared storage assets The potential for interaction of increased pressure at multiple injection sites needs to be predicted and assessed at a regional scale to assure the integrity at all existing sites before a storage permit is granted. Geomechanical models coupled with the expected fluid pressure response predict the stability of the storage asset during and after injection of CO_2 at multiple injection sites, and can be used as a tool to ensure efficient utilisation of the storage capacity. The geomechanical analysis of the thermal stress as well as local and regional fluid pressure changes requires a detailed numerical evaluation, often at a resolution significantly higher than the data available. Coupling of regional-scale static geological models, dynamic multi-phase flow models and detailed geomechanical models requires extensive computational resources. Such models often produce seemingly detailed results, but are usually only one or two realisations of a system populated by a statistically generated parameter set. Limits on time and computational resources prevent more simulations within fixed time and financial budgets. To enable a more time and cost efficient methodology of assessing the geomechanical stability of potential storage sites we present a four-tier modelling approach with increasing complexity that allows an in-depth evaluation of the geomechanical stability at a regional scale of a multi-user storage asset taking into account the fluid pressure increase and the thermal stress impact on the stability of the strata sealing the CO_2 store. The tiers include (1) development of a geo-mechanical facies model of the storage system, (2) development of an analytical geomechanical model for the storage site static stress conditions, (3) fitting an empirical multivariable polynomial function to the analytical modal, and (4) conditioning the empirical function using coupled numerical THM modelling for dynamic stress conditions. The result is look up function which gives the maximum possible fluid pressure as a function of location. This approach significantly simplifies the computational requirements and time for the prediction of geomechanical behaviour. In addition to presenting this methodology, using the Captain Sandstone of the North Sea as an example, three key findings are further examined. Firstly, detailed analysis of

the stress changes as a result of cold fluid injection suggests that the redistribution of thermal stress can, in some cases, be beneficial to the storage system depending on the stress bridging which occurs. Secondly, pressure plume migration over time in dipping strata, from deeper injection sites to shallower sites, needs to be taken into account. Thirdly, the nature of the strata underlying the storage formation is critical to the pressure increase in response to the fluid injection. The methodology developed in this paper enables a rapid and efficient screening of the dynamic geomechanical stability and an efficient coupling to diverse discrete multiphase fluid flow models using commonly available computational resources.

Key Words

Geomechanical simulation, scCO2 storage, Reservoirs, Rock mechanics, THM numerical modelling, Screening tool

Introduction

Carbon capture and storage permanently stores CO_2 captured at large-scale industry and power plants to significantly reduce the emission of anthropogenic waste CO_2 to the atmosphere, and address one of the key concerns regarding global climatic change. Sovereign countries and competent authorities that possess and regulate large commercially attractive offshore resources are increasingly aware of the need to manage the storage of CO_2. Such storage resource assets need to be managed with a joined-up approach, and not just an unsustainable exploitation of 'what is possible and cheapest now', to optimise potential storage capacity. Failure to do so could lead to a reduction in the usable storage capacity, due to store integrity constraints, and significant long term deterioration in the asset value. The challenge will increase where the strata used for multiple injection sites extend across international borders.

Given the extent of regional storage formations, it is expected that multiple injection sites will operate to exploit the same contiguous and hydraulically connected pore space. Competition for the storage capacity asset should be expected; without effective pressure management even relatively small volumes of stored CO_2 can have a significant impact on the regional fluid pressure within the storage formation. Additionally, the maximum acceptable pressure values predicted by geo-mechanical modelling do not display a linear relationship with the depth of the storage formation. In dipping strata long-term migration of increased pressure to shallow areas, which may be at some distance from the CO_2 injection points, may determine the maximum acceptable pressure at deeper parts of the formation.

In this paper a generic methodology is presented enabling the geomechanical stability of a storage site to be relatively rapidly assessed at a regional scale. The methodology develops a "look up" function (location dependent) enabling geomechanical pressure limits to be transferred simply from one simulator to another. The methodology is developed on and applied to the Captain Sandstone in the North Sea (Figures 1 and 2) (Kopervik Fairway of Law et al., 2000). This is assessed as a potential multi-user store as it is a preferred site for a UK demonstrator project for geological CO_2 storage (DECC, 2013). The geomechanical impact of the injection of commercially viable storage volumes of dense supercitrical (sc) phase CO_2 into the Captain Sandstone was investigated at two realistic locations: Site A in the vicinity of the Goldeneye Gas Field; Site B in brine-saturated Captain Sandstone approximately forty kilometres up-dip of Site A(Figure 1).

Predictive modelling of potential pressure changes within the storage formation to ensure prospective storage operations are within the acceptable geomechanical limits requires the use of numerical multi-physics models. Such models enable assessment the efficient utilisation of the available storage capacity. These models require reliable geological, fluid flow and geomechanical information. Information is needed on a regional scale for the strata present, and this needs to be discretised to sufficient detail that reasonable geometrical models of the injection sites can be

92 constructed, and an acceptable parameterisation of the strata undertaken. The parameterisation
93 needs to address all the values required for the multi-physics simulation of the system.

94 There are several simulators, and combination of codes, that allow simultaneous evaluation of the
95 fluid flow and the geomechanical response, e.g. Magri et al. (2013), Rutqvist et al. (2006), Rutqvist et
96 al. (2002). However multi-physics problems generally require data at several different scales of
97 resolution, particularly where discrete features such as faults in the geomechanical analysis are
98 taken into account e.g. Cappa and Rutqvist (2011), Vidal-Gilbert et al. (2009). The scale and
99 availability of data required in the different simulations means that efficient methods are required to
100 integrate the results of one part of the simulation with another.

101 The geomechanical modelling requires both detailed representation of the area around the injection
102 wells where the impact of the thermal signal is to be taken into account, and also a regional
103 representation of the strata to account for the large areal extent of a possible pressure increase. In
104 this study the impact of the thermal stress around the injection well was evaluated using a grid size
105 of the order of a few metres, whereas the geological heterogeneity recorded in the horizontal
106 dimension within the storage formation was approximately 250 metres.

107 Parameterisation of numerical models of regional extent is usually based upon a statistical approach
108 with data taken from relatively few selected boreholes. The resolution achieved here of 250 metres
109 is more finely scaled than usually available, which is normally in the order of 500 metres or more.
110 The data is typically presented as a probability distribution function rather than a true kriged
111 statistical analysis as there is not sufficient confidence in the evaluation of the correlation of the
112 parameters with geometrical location. A normal, or log normal, distribution approach to the
113 evaluation of the material characteristics can be expected to capture the behaviour of the system as
114 a whole. However, any single realisation of the statistical field is just one representation of a wide
115 range of equally valid possibilities. Usually, modelling is constrained by the computational power and
116 time needed to run multiple simulations.

117 Here we present a four-tier modelling approach, applied to the Captain Sandstone offshore
118 Scotland, to evaluate the geomechanical stability of a multi-user store to CO_2 injection as a
119 consequences of multiple sites of injection, covering both thermal effects near the well and regional
120 pressure build up. The tiers include (1) development of a geo-mechanical facies model of the storage
121 system, (2) development of an analytical geomechanical model for the storage site static stress
122 conditions, (3) fitting an empirical multivariable polynomial function to the analytical model, and (4)
123 conditioning the polynomial function using coupled numerical THM modelling for dynamic stress
124 conditions along a number of cross sections. Tier (4) results in a depth, and where relevant, location,
125 dependent look up function which is easily transferable to other simulators.

126 Three key findings are also examined here. Firstly, detailed analysis of the stress changes as a result
127 of cold fluid injection which suggests that the redistribution of thermal stress can, in some cases, be
128 beneficial to the storage system depending on the stress bridging which occurs. Secondly, pressure
129 plume migration in dipping strata from deeper injection sites to shallower sites over time needs to
130 be taken into account. Thirdly the nature of the strata underlying the storage formation is critical to
131 the pressure increase in response to CO_2 injection.

132

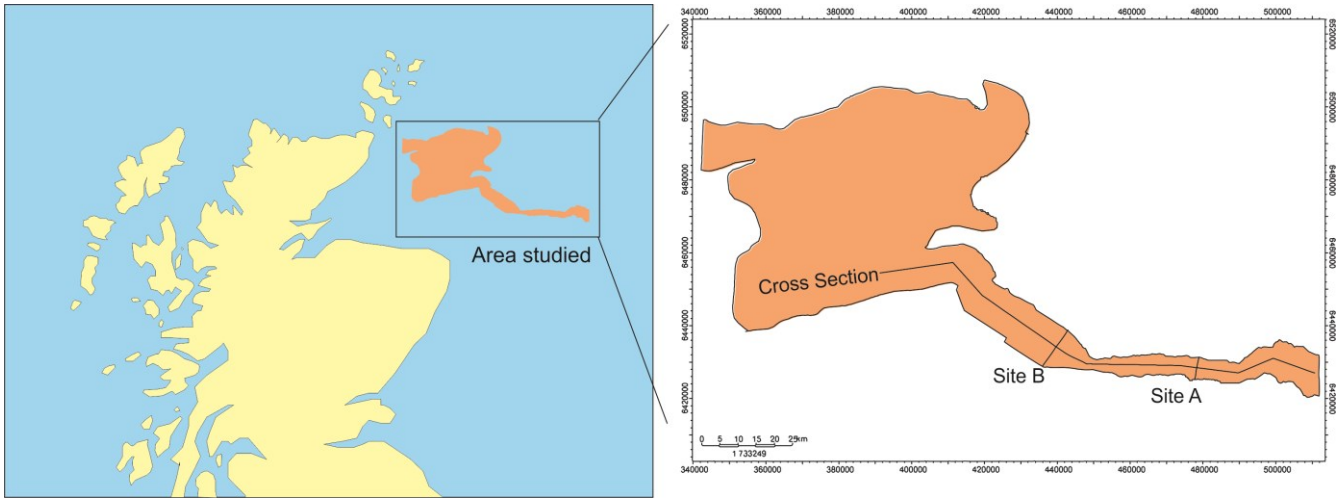

Figure 1 Location of Captain Sandstone offshore Scotland, northern North Sea (left) and extent of area studies (inset right).

Method

The geomechanical modelling is of a volume of the Captain Sandstone where it is narrowed and is termed the Captain Sandstone Fairway, indicated by the location of the cross-section in Figure 1. We develop a four tier modelling approach of increasing complexity to the evaluation of the geomechanical stability of the Captain Sandstone Fairway during the proposed injection of the CO_2. The result is a portable empirical function based on detailed geomechanical modelling which can be used to predict maximum possible safe fluid pressures within the Captain Sandstone Fairway.

- Tier 1: Development of a conceptual geomechanical facies model
- Tier 2: Development of an analytical geomechanical model for static conditions
- Tier 3: Fitting Tier 2 with an empirical polynomial function
- Tier 4: Application of 2D and 3D multi-physics coupled process models to refine the Tier 3 polynomial function to include dynamic stress conditions and resulting in the location dependent look up function.

The result from Tier 4 is a spatially correlated estimation of the maximum overpressure possible within the storage strata, including both the reservoir (principal storage location), primary seal and secondary seal. Each of these Tiers are described here and discussed in more detail later.

The first Tier comprises assessing the geological information on the storage complex (as defined in EU, 2011) and developing a geomechanical facies model of the system. The geomechanical facies model provides the basis for the further modelling investigation and parameterisation of the system (Edlmann et al. 2014; McDermott et al. 2006a; Tenzer et al. 2010).

The second Tier uses an analytical approach for static stress conditions prior to dense phase CO_2 injection to evaluate maximum fluid pressures possible in the storage complex. The analytical modelling provides a generic approach to the evaluation of the stability of a rock unit as a function of the poly axial stress, fluid pressure and rock mechanical parameters. Possible failure mechanisms of the rock at this level include tensile failure, shear failure and reactivation of existing planes of weakness. At this level as much available data as possible is included in terms of stress profile from field measurements and laboratory results of solid, fluid and medium properties. The analytical solution provides a reference value for the maximum fluid pressures which can be contained, but does not take into account local heterogeneity (different thicknesses of strata, parameter variations), the impact of thermal stress or the dynamic impact of the increase in the fluid pressure and consequent reduction in horizontal stress within the storage complex.

The third Tier is to develop an empirical multivariable polynomial function which provided the maximum possible fluid pressure in the storage complex predicted by Tier 2 as function of depth and

location (primary seal, secondary seal or faulting). This was refined in Tier 4 to include the dynamic stress conditions, heterogeneity and thermal stress.

The forth Tier of evaluation was to employ fully coupled thermal hydraulic mechanical (THM) multi-physics code at a number of selected locations throughout the Captain Sandstone. The coupled process finite element simulator, OpenGeosys, (Kolditz et al. 2012) was further developed to include standard rock mechanical stability analysis. This was then used to simulate a large scale 3D model (HM), approximately 130 by 20 kilometres, and selected high resolution 2D (THM) cross sections (mesh resolution to ten metres) to evaluate the maximum safe dynamic fluid pressure in the Captain Sandstone. The 3D model provided realistic estimates of the changes in fluid pressure expected during the injection of commercial-scale volumes of CO_2 (6million tonnes (Mt) per year at each site). The predicted fluid changes in the 3D model were then used to define the source terms and pressure changes expected in the 2D detailed resolution models (2D THM). The same failure mechanisms included in the Tier 2 model were included in the 2D THM numerical models. These models enabled local heterogeneity in terms of the different thicknesses of strata to be included, the impact of thermal stress to be assessed and the dynamic impact of the increase in the fluid pressure and reduction in horizontal stress to be taken into account.

The results of the third Tier empirical function were then compared with the results of the forth Tier dynamic THM modelling results. The empirical function was refined with a correction factor to match the fourth Tier results, i.e. include the dynamic modelling results. The correction factor could also takes into account the location in terms of defining a zone of possible influence of the thermal stress around the injection sites, the presence of fault zones and which strata the analysis was in (primary seal, secondary seal). The augmented empirical fit then provides a depth and location dependent maximum safe fluid pressure throughout the Captain Sandstone Fairway and sealing strata. This function can then be ported to be used in detailed multiphase fluid pressure simulations as a simple look up function approach providing coverage for the whole of the Captain Sandstone Fairway. The depth and location dependent function provides a numerical summary of the detailed geomechanical simulations.

Model assumptions

A modelling approach provides a mathematical approximation of reality and a tool for estimating the behaviour of the system based on known processes. Simplification of the system needs to be undertaken whereby the main processes operating are captured. The model requires simplifications in terms of the geometry of the deposits, the range of parameters assigned to the deposits, the discretisation of the heterogeneities both within strata and between strata, the fluid properties, and the processes to be included. In précis four assumptions on the behaviour of the system were applied to simplify the modelling approach;

Assumption 1: Fluid flow and pressure build up can be satisfactorily modelled as single-phase flow. This assumption was based on the facts that the reservoir temperature is of the order of 83 °C in the storage asset, and so the viscosity of brine at this temperature is approximately 0.0004 Pa s. $scCO_2$ injected at 20°C has a viscosity of circa 0.0001 Pa s. Therefore, the overall control on the pressure build up around the injection well will be that of the mobility of the far-field brine and not the CO_2 in the vicinity of the well. Thermal calculations show that a significant temperature effect generated by CO_2 injection is localised to <1km after 30 years. The advantage that this assumption has is that a multiphase flow simulation would require significantly more computational resources, as well as several further parametrical modelling assumptions such as capillary entry pressures, relative permeability curves and hysteresis behaviours of wetting and non-wetting fluids. Therefore this assumption significantly simplifies the computational resource required.

Assumption 2: The model was populated with mean parameters for strata layers and the layers considered to be homogeneous and isotropic. This approach was based on the nature of the data available. The grid spacing of geometrical and geological data was resolved down to 250m

horizontally, and metre-scale vertically. The geometry and structure of the strata were taken from cross-sections from the static geological CO2MultiStore Captain Sandstone model (Figure 1). The heterogeneity of the different layers is known stochastically and not discretely.

Assumption 3: The mechanical response of the system was modelled for elastic conditions only. Plastic deformation was not considered.

Assumption 4: Fluid flow out of the model may occur within the Captain Sandstone Fairway to the south east and north west, it does not occur to adjacent lateral strata, it may or may not occur through the base of the underlying strata. Identifying realistic boundary conditions (for both the hydraulic and the mechanical model) is key to successfully calibrating the modelling approach. In general, the lateral boundaries of the Captain Sandstone Fairway were considered to be closed to fluid flow as the geology showed there was no extension of the Captain Sandstone beyond the limits of the Fairway. The lateral boundaries were also assumed to be ridged. This was based on the fact that there was little information available on the nature of the material beyond the boundaries of the Captain Fairway and it was clear that an assumption of unrestrained boundaries was not valid. Assuming ridged lateral boundaries, so that any lateral boundary deformation is not accommodated by strain, leads to a worst case assumption in terms of stress build up, but therefore a safer analysis of the impact on the integrity of the strata due to possible overpressure build up due to CO_2 injection in the strata. The base of the model was considered immobile. The top surface was considered open to fluid flow, at constant temperature and able to deform.

One of the most important assumptions proved to be the type of fluid flow boundary for the base of the model. Two boundaries types were considered to give “end member” results. First at the base of the model an open flow boundary was considered where the pressure release from the model through the base was dictated by a layer of strata circa 800 metres thick with a permeability representative of this strata, and secondly a no flow fluid boundary at the base of the model.

The choice of the base of the model as a constant hydrostatic fluid pressure boundary allows excess pressure in the reservoir to be released through the under lying strata (the Underburden). The Underburden defined in the geomechanical model comprises a stratigraphic sequence of sedimentary deposits including mudstone and sandstone down to strata of Permian age. The Jurassic sequence comprises the Kimmeridge Clay and sandstone, beneath which are volcanic rocks. These are underlain by mudstone and sandstone of Triassic age that overlie strata of Permian age marked by evaporate deposits of the Zechstein Group. This Jurassic to Permian sequence can be several kilometres in thickness, and only at the Zechstein evaporite deposits can we be sure that there is a no-flow boundary. Choosing the base of the model to be impermeable means that the pressure release from injection into the sandstone can only occur either through the seal rocks or through the open edges of the model (farther north westwards and farther south eastwards where the Captain Sandstone Fairway is known to extend further). The assumption of the lower boundary of the Underburden being closed to flow leads to significantly higher pressures being built up in the reservoir than if the lower boundary of the underburden allows some pressure release. In addition it leads to increased pressure communication between the separate injection sites.

Tier 1: From geology to geomechanical facies

A brief overview of the geology of the Captain Sandstone Fairway is presented as a stratigraphic column in Figure 2. A cross section of the Captain Sandstone Fairway is presented in Figure 3, the location of the cross section is illustrated in Figure 1. The uppermost strata comprise the recent deposits of the Nordland Group, underlain by Tertiary strata of the Moray Group and the Montrose Group. These are variously inter-bedded cohesive and non-cohesive units, with a thickness in the Captain Sandstone Fairway of several hundreds of metres. At the base of the Cenozoic deposits the youngest chalk interval is the Ekofisk Formation. The Upper Cretaceous succession comprises the Tor, Mackerel and Herring formations. Within this group there are occasional mudstone units which

are considered to be sealing. These are found towards the east of the Captain Sandstone Fairway, with a thickness of the order of 500 metres, to the west they can be absent. Within the base of the Herring Formation the Plenus Marl overlies the Hidra Formation. The Plenus Marl and the Hidra Formation are composed of relatively ductile shale and marl. They form part of the primary seal (caprock) to the Captain Sandstone in conjunction with the underlying Rodby and Carrack formations. The total thickness of these strata can be of the order of 200 metres. However, in some areas it is known that the Rodby and Carrack formations are not present. Beneath these low permeability rocks is the Captain Sandstone (a member of the Wick Sandstone Formation).The Captain Sandstone is informally subdivided into an Upper Captain Sandstone Unit, the Mid Captain Shale, and the Lower Captain Sandstone. The Lower Captain Sandstone is ubiquitous throughout the study area, the Uppermost Captain Sandstone is absent to the west of the area and over the Captain Ridge (Pinnock et al. 2003). The Captain Sandstone is usually of the order of 100 metres thick. However, in some areas the lower Captain Sandstone can be two or three times this thickness. The Captain Sandstone is laterally equivalent to the Valhall Formation which is underlain by the Humber, Fladen and Heron groups. The Humber and Heron comprise various sedimentary strata and the Fladen group comprises volcanic deposits forming the Jurassic and Triassic succession. The underlying Zechstein Group marks the top of Permian strata and an impermeable base including a number of evaporite deposits. The combined thickness of the Humber and Heron groups is of the order of several kilometres.

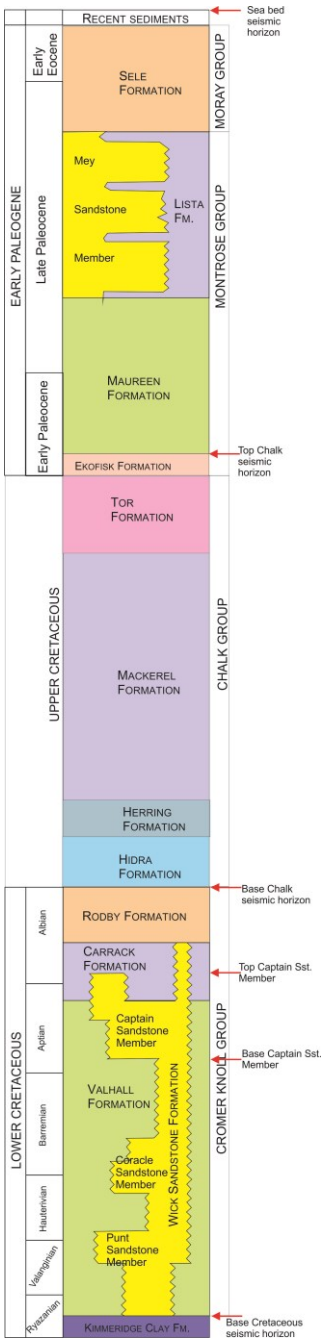

Figure 2 Generalised stratigraphy profile of the study area, from the BGS, Johnson and Lott (1993) and Knox and Holloway (1992), reproduced from SCCS (2011).

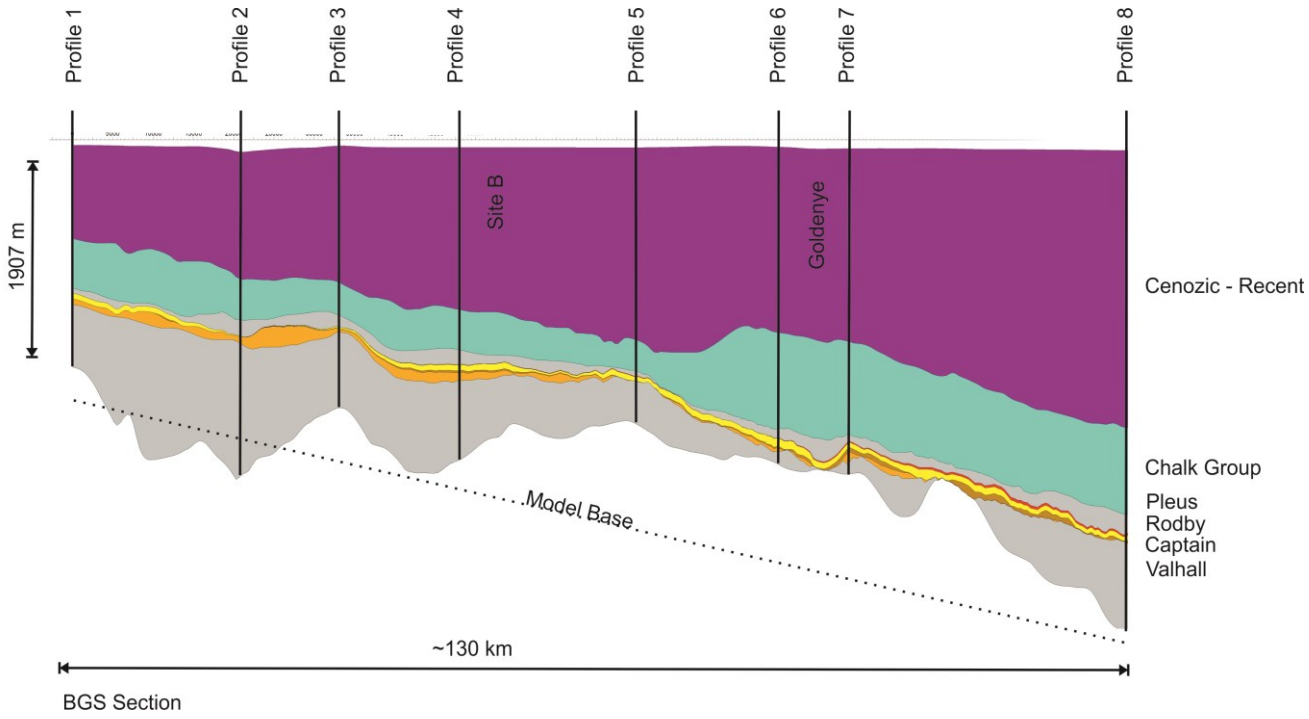

Figure 3 Geological cross-section of the Captain Sandstone Fairway. Line of cross-section shown in Figure 1. Numbered profiles selected for construction of the 3D geomechanical model as marked (SCCS 2015).

Table 1 Profiles and depths of strata

	Profile 1	Profile 2	Profile 3	Profile 4	Profile 5	Profile 6	Profile 7	Profile 8
Distance from west (m)	0.00	21000.00	33200.00	48000.00	70000.00	87600.00	96500.00	122300.00
X Coordinate (m)	0.00	20185.04	31278.53	43930.97	64675.98	83032.22	92080.20	118555.24
Y Coordinate (m)	33944.48	35860.16	25085.75	16225.53	8683.17	7937.83	7054.72	6244.38
Top of Overburden (m)	-89.91	-148.64	-106.97	-121.74	-124.46	-122.34	-132.04	-144.96
Top of Secondary Seal (m)	-854.73	-1202.99	-1230.43	-1461.32	-1705.97	-1647.65	-1743.91	-2439.41
Top of Primary Seal 2 (m)	-1212.96	-1473.68	-1435.09	-1714.25	-1902.58	-2284.43	-2375.33	-3050.18
Top of Primary Seal 1 (m)	-1265.22	-1531.37	-1498.32	-1781.02	-1960.86	-2451.34	-2495.69	-3152.39
Top of Reservoir (m)	-1321.39	-1652.41	-1597.72	-1906.36	-2008.38	-2524.80	-2556.16	-3316.58
Top of Underburden (m)	-1407.80	-1760.45	-1645.26	-2036.00	-2055.92	-2637.13	-2703.08	-3398.69
Base of Underburden (m)	-2207.80	-2560.45	-2445.26	-2836.00	-2855.92	-3437.13	-3503.08	-4198.69
Interpreted top surface (m)	-89.91	-105.44	-103.00	-103.39	-110.52	-122.34	-127.68	-144.96
Interpreted surface base (m)	-2207.80	-2712.42	-2694.33	-2759.32	-3040.37	-3437.13	-3619.82	-4198.69

For the evaluation of the storage of CO_2 in the subsurface it is necessary to consider the behaviour of different strata as a response of their material characteristics in terms of the key processes considered. To do this the profile is divided into key geo-mechanical facies comprising a passive overburden, an active (sealing) overburden, the storage reservoir sandstone and the underburden (Edlmann et al. 2014). The term geo-mechanical facies expresses the fact that different geological units can be grouped together in terms of their material behaviour (fluid and mechanical behaviour) and perceived role in an applied engineering application. The geo-mechanical facies may contain different geological units, but as a group have a distinct role in terms of engineering application, in this case CO_2 containment at depth. For the Captain Sandstone Fairway we identify five geomechanical facies, the Reservoir, the Underburden, the Primary Seal, the Secondary Seal and the Passive Overburden.

The “Reservoir ” geomechanical facies is the group of generally relatively high porosity and permeability geological units into which the CO_2 is being injected and where, through a variety of processes, the CO_2 is to be stored (members of the Wick Sandstone Formation, Figure 2). The “Underburden” geo-mechanical facies comprises those strata underlying the base of the reservoir (Figure 2) and also the underlying lithostratigraphical units (Humber, Fladen, Heron and Zechstein

groups, Table 2). The Underburden is usually taken to be passive in terms of its influence on the storage formation. However through this modelling investigation we show that the nature of the Underburden significantly effects both the storage capacity and the sealing capacity of the system. The active sealing overburden, or caprock, and other sealing members comprise units capable of resisting fluid flow over thousands of years and provide mechanical restraint and sealing to the build-up of fluid pressure in the reservoir as a result of the injection of CO_2. In this case two "Primary Seals" and a "Secondary Seal" are identified. The "Passive Overburden" comprises strata not contributing to the fluid sealing capacity of the reservoir but providing support to the sealing layers through its weight. For the Captain Sandstone Fairway the five geomechanical facies identified are listed in Table 2 below.

Table 2 Division of strata into geomechanical facies.

Geomechanical Facies	**Members**
Passive Overburden,	Recent formations of the Norland Group Cenozoic formations of the Moray Group and the Montrose Group.
Secondary Seal	Upper Cretaceous and Lower Tertiary formations of the Chalk group, that is the Ekofisk Formation, the Hod Formation, the Mackerel Formation and the Herring Formation excluding the Plenus Marl at the base.
Primary Seal 2 Primary Seal 1	Plenus Marl Hidra Formation Rodby Formation Carrack Formation.
Reservoir	Comprising the Captain Sandstone and other members of the Wick Sandstone Formation.
Underburden	The Valhall Formation below the Captain Sandstone, the Humber Group, the Fladen Group and the Heron Group assumed to extend to the Zechstein Group at the top of the Permian.

Tier 2: Applying an analytical geomechanical model for evaluating stability under static stress conditions

During injection of CO_2 into the reservoir, two regimes can be identified; the near-field and the far-field. The near-field effects are caused by a sharp change in the spatial gradients of field variables of temperature, fluid pressure, and rock stress. In the case of fluid injection there is a sharp increase in fluid pressure in the vicinity of the injection well. Likewise in the case of a thermal effect, there is an abrupt change in the temperature in the vicinity of the injection well. In the far field there is a general gradual increase in fluid pressure.

Increasing the fluid pressure or changing the temperature of a rock can lead to the development of new fractures or movement along a pre-existing fracture plane. This leads to a change in the geometry of the material and a change in the medium properties of the material. Generally such changes will accommodate fluid flow through the material as a means of reducing and relieving the increased pressure or thermal stress placed on the material. This failure will lead to the function of the geomechanical facies being impaired should its main role in an engineering sense be the

retention of fluids, stored CO_2 in this case. Whether a facies is stable or likely to fail depends on the stress on the facies and some characteristic geomechanical parameters described below.

In our assessment of the stability of the primary and secondary seals, we took into account tensile failure, rock fracturing and movement along a pre-existing fracture planes. Several text books deal with the methods of calculating tensile, shear and normal stress e.g. Jaeger et al. (2007). Orientating the axis such that the principle stresses line up with the axis x,y,z we can write for the normal stress across the plane σ_n (Pa)

$$\sigma_n = l^2\sigma_v + m^2\sigma_H + n^2\sigma_h \quad \textbf{(1)}$$

where l is the directional cosine for the angle between the normal to the plane and the vertical principal stress axis, m and n likewise for the horizontal stress axes. And for the shear stress parallel to the plane, τ, we can write

$$\tau = \sqrt{\left(l^2\sigma_v{}^2 + m^2\sigma_H{}^2 + n^2\sigma_h{}^2 - \sigma_n{}^2\right)} \quad \textbf{(2)}$$

The relationship between the maximum shear stress, or the shear stress which will cause failure τ_f and the normal stress across a plane is given by

$$\tau_f = c + \left(\sigma_n - \alpha u\right)\tan\phi \quad \textbf{(3)}$$

where ϕ is the angle of friction of the failure plane, c represents the cohesive strength of the rock or plane and u is the fluid pressure (Pa). The amount of pressure transferred from the pore or fracture space to the skeleton can be expressed in its simplest form above with the Biot Willis coefficient, α, a ratio of fluid pressure to transferred rock pressure.

For intact rock, cohesion can be calculated from the standard rock parameter the Unconfined Compressive Strength $\left(UCS\right)$ as

$$c = \frac{UCS\left(1-\sin\phi\right)}{2\cos\phi} \quad \textbf{(4)}$$

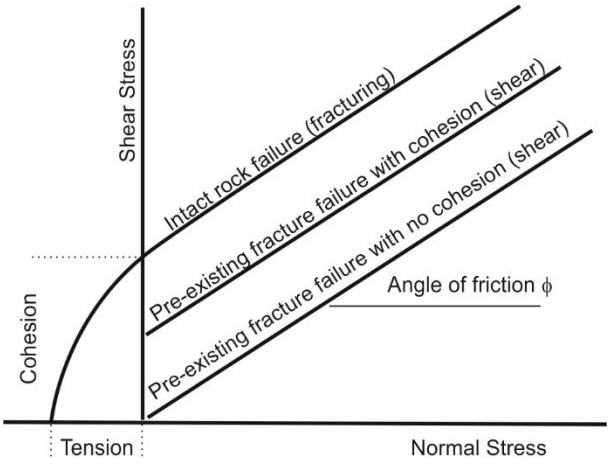

Figure 4 Typical characteristics of rock failure

The impact of thermal stress on the effective stress can also be evaluated such that

$$\boldsymbol{\sigma}' = \boldsymbol{\sigma} + \mathbf{Kr}\beta\mathbf{E}\Delta T \quad \textbf{(5)}$$

Where ΔT (K°) is a temperature change in degrees kelvin, Kr (-) is a coefficient of restraint e.g. (McDermott et al. 2006b; Tenzer et al. 2010), β is the thermal expansion coefficient (K^{-1}) and $\mathbf{E}$ is the elastic modulus of the rock. Cooling is approximately isotropic, and likewise the elastic properties of the material in the reservoir are assumed isotropic. Heterogeneity can be seen at a larger scale considering the layered nature of the storage system, and this will be revisited later. Assuming full restraint in all directions the general impact of the thermal stress is to augment the impact of the increase of fluid pressure and move the Mohr's circles further to the left, and closer to the failure envelope. Under certain heterogeneous conditions however the superposition of the thermal stress, and an effect known as stress bridging can be shown to increase the confining stress.

The likelihood of the rock failing under a given stress regime can be expressed by a factor of safety. The factor of safety F is the ratio of disturbing forces to restraining forces. When the value is 1 or less a breach in the strata can be assumed to have occurred.

$$F = \frac{\tau_f}{\tau} \quad \textbf{(6)}$$

In engineering terms if F is larger than 1 then there are more restraining forces than disturbing forces. Usually during engineering design for construction a Factor of Safety of at least 1.3 is required. For critical works a higher value may be required.

Where the slip plane is not already determined by the presence of a discontinuity, the safety of the orientation most likely to fail needs to be evaluated. To do this the principal stress directions need to be calculated taking into account the superposition of thermal stress, fluid stress and rock stress which can lead to rotation of the principal stress axis away from the chosen coordinate system. If the direct stresses and shear stresses in a particular coordinate system are known the orientation and size of the principal stresses can be calculated as follows (Lewis and Schrefler 1998)

$$p = -\frac{1}{3}\left(\sigma_x + \sigma_y + \sigma_z\right) \quad \textbf{(7)}$$

$$q^2 = \sigma_x\left(\sigma_x - \sigma_y\right) + \sigma_y\left(\sigma_y - \sigma_z\right) + \sigma_z\left(\sigma_z - \sigma_x\right) + 3\left(\tau_{xy}^2 + \tau_{yz}^2 + \tau_{zx}^2\right) \quad \textbf{(8)}$$

$$\theta = \frac{1}{3}\sin^{-1}\left[-\frac{27J_3}{2q^3}\right] \quad \textbf{(9)}$$

$$J_3 = \begin{vmatrix} \sigma_x + p & \tau_{xy} & \tau_{zx} \\ \tau_{xy} & \sigma_y + p & \tau_{yz} \\ \tau_{zx} & \tau_{yz} & \sigma_z + p \end{vmatrix} \quad \textbf{(10)}$$

The three principal stresses at any location are then evaluated as

$$\begin{pmatrix} \sigma_1 \\ \sigma_2 \\ \sigma_3 \end{pmatrix} = \begin{pmatrix} p \\ p \\ p \end{pmatrix} - \frac{2}{3}q \begin{pmatrix} \sin\left(\theta - \frac{2}{3}\pi\right) \\ \sin\theta \\ \sin\left(\theta + \frac{2}{3}\pi\right) \end{pmatrix} \quad \textbf{(11)}$$

Following this the factor of safety for a rock unit can be expressed as

$$F = \left(\frac{c}{\cos\phi} + \left(\frac{(\sigma_1 + \sigma_3)}{2} \right) \sin\phi \right) \Big/ \frac{(\sigma_1 - \sigma_3)}{2} \qquad (12)$$

For the case where there is a plane of given orientation, such as a fault or a pre-existing fracture plane, the fluid pressure likely to cause failure on this plane can be evaluated. From (1) and (2) the normal stress σ_n and the shear stress τ are known, by rearranging (3) we can show that the minimum fluid pressure which will cause shear u_f will be

$$\frac{\tau - c}{\tan\phi} - \sigma_n = -u_f \qquad (13)$$

One further constraint on fluid pressure is that it may not exceed the horizontal stress. Using the above equation it is possible to find an orientation where the rock will not slip as it is being held together by cohesive forces, but the fluid pressure is higher than the horizontal stress. In this case we assume a default safety consideration that the rock does not exhibit tensile strength and that failure will occur.

Data Sources and Parameter Selection

Hydraulic, thermal and mechanical parameters were collected from a number of sources (Scottish Power CCS Consortium 2011a,b,c, Chang et al. 2006, and references therein). Where data was not available then typical literature values of those parameters were assigned. An overview of the parameters is given in Table 3.

Table 3 Overview of Hydraulic, Thermal and Mechanical Parameters Selected for THM Simulation of the Captain Sandstone Fairway

		Hydraulic Parameters			Mechanical Parameters, Worst Case				Mechanical Parameters, Reasonable			
Formation	Geomechanical Facies	Porosity n	Permeability k	Storage S (1/Pa)	Cohesion c (MPa)	Friction Angle ϕ°	Elastic Modulus E (GPa)	Poisson's ratio v	Cohesion c (MPa)	Friction Angle ϕ°	Elastic Modulus E (GPa)	Poisson's ratio v
Norland Coals Dornoch	Passive Overburdan	0.31	152mD	2.08E-10	10	10	3	0.46	10	10	3	0.46
Chalk Group	Secondary Seal	0.06	0.63nD	4.97E-11	0	28	30	0.32	0	28	30	0.32
Rodby Carrack Plenus Hidra	Primary Seal 1 Primary Seal 2	0.06	0.15nD	7.98E-11	0	13	10	0.38	6	13	10	0.38
Captain	Reservoir	0.2	613mD	1.30E-10	0	20	20	0.25	3	34	20	0.25
Valhall Humber Heron	Underburdan	0.09	9.25mD	7.67E-11	10	20	20	0.3	10	20	20	0.3

Thermal Parameters		
Thermal expansion coefficient	1.10E-05	
Thermal conductivity of rock	3	W/m°K
Heat capacity of rock	1000	J/kg°K
*Density of formation	2550	kg/m³
**Reservoir Longtitudinal Heat Dispersivity	5	m
**Reservoir Transverse Heat Dispersivity	5	m
Fluid Heat Capacity	4280	j/kg
Fluid Heat Conductivity	0.6	W/m°K
Reservoir temperature	83	°C
Sea bed temperature	5	°C

Fluid hydraulic parameters		
Fluid Viscosity	0.0004	Pa s
Fluid Density	1019	kg/m³
Average salinity	19	g/l
Other contants		
Biot Willis Coefficient	1	

*Calculation of initial stress state =f(depth), see text.
**See text

The permeability and porosity of the geomechanical facies were derived from the static geological model. The values provided by this report were converted into effective permeability whereby

$$k = k_{BGS} NTG \quad \textbf{(14)}$$

Where the NTG is the Net sandstone To Gros thickness ratio, representing the volumetric ratio of the cells open to fluid flow, k_{BGS} is the mean permeability value, and k is the effective permeability of the cells for numerical modelling.

The compressibility C_m (Pa^{-1}) of a rock unit is given by

$$C_m = \frac{1}{E}\frac{(1-2v)(1+v)}{(1-v)} \quad \textbf{(15)}$$

The specific storage Ss (Pa^{-1}) is given by

$$Ss = (C_m + nC_w) \quad \textbf{(16)}$$

The calculation of the storage parameters is given in Table 4. The compressibility of fluid (brine is assumed as this is being forced out of the way to accommodate the CO_2) is $4.4\times10^{-10}\ Pa^{-1}$. The NTG ratio is not taken into account in the storage calculation as we assume the whole geological unit will experience the stress changes due to fluid injection.

Table 4 Calculation of specific storage parameters

	Passive Overburden	Secondary Seal	Primary Seal	Reservoir	Underburden
n (Porosity)	0.31	0.06	0.06	0.20	0.09
v (Poisson's ratio)	0.46	0.32	0.38	0.25	0.30
E (Youngs Modulus) Pa	3.00E+09	3.00E+10	1.00E+10	2.00E+10	2.00E+10
Ss (Specific storage) Pa^{-1}	2.08E-10	4.97E-11	7.98E-11	1.30E-10	7.67E-11

Shell (2011a) report a thermal expansion coefficient of the order of $1.1\times10^{-5}\ K^{-1}$ which is at the higher end of what would be expected, but not unreasonable.

Values commonly found in the literature were assumed for the rock thermal conductivity, fluid thermal conductivity, specific heat capacity of rock, specific heat capacity of water. Approximating the injection of $scCO_2$ using single phase brine flow will lead to an overestimation of the impact of the thermal pulse. The heat dispersion diffusion coefficient is taken to be approximately one half the mesh spacing for stability reasons. The use of the heat dispersion diffusion coefficient represents mixing and spreads the front of the heat signal out.

Stress Profile and Temperature Gradient

A hydrostatic pore pressure gradient of 10 kPa/m has been measured in the formations below the reservoir, to a depth of circa 3000 m, Shell (2011b). This equates to an average pore fluid density of 1019.4 kg/m^3. The pore fluid pressure at any depth is then given by (17), where z is depth below surface, and g is the acceleration due to gravity = 9.81 m/s^2.

$$u = 1\times10^5 + 1019.4zg \quad \textbf{(17)}$$

From the Shell pore pressure prediction report (Shell 2011b) the minimum horizontal total stress is given as

$$\begin{aligned} \sigma_3(psi) &= 0.421 * TVDSS(ft)^{1.049} && < 6000\,ft \\ \sigma_3(psi) &= 0.0067 * TVDSS(ft)^{1.5254} && > 6000\,ft \end{aligned} \quad \textbf{(18)}$$

where TVDSS is True Vertical Depth Sub Sea level. These can be expressed in (m) and (MPa) as

$$\begin{aligned} \sigma_3(MPa) &= \left(0.421 * TVDSS(c_1 z(metres))^{1.049}\right) / c_2 && < 1828m \\ \sigma_3(MPa) &= \left(0.0067 * TVDSS(c_1 z(metres))^{1.5254}\right) / c_2 && > 1828m \\ c_1 &= 3.2808399 \quad c_2 = 145.0377 \end{aligned} \quad \textbf{(19)}$$

The shell profile for total minimum horizontal stress has been derived as far as possible from the lower margins of the possible Leak Off Test data available.

The vertical total stress profile is given as

$$\sigma_v = -0.4545 + 0.0204z + 9.0043e-7z^2 \quad \textbf{(20)}$$

The thermal gradient was estimated for the storage complex, with the reservoir at a depth of 3000 m taken to be at a temperature of 83°C, and a sea floor temperature of 5°C. The initial conditions summarized above are illustrated below in Figure 5

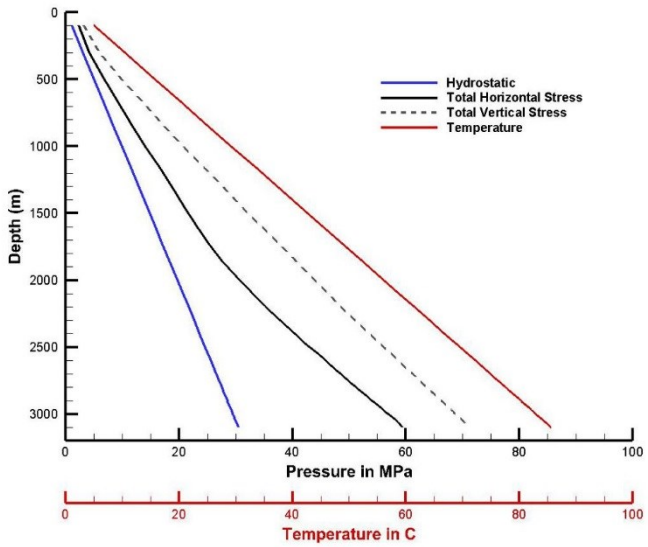

Figure 5 Initial conditions assumed in the storage complex

The assumptions about the mechanical failure parameters of the different geomechanical facies can be tested using a model relating the normal stress, the shear stress and the failure parameters of the unit to the expected in situ stress. Equation (13) provides the relationship between these parameters, and the equations (1) and (2) describe how the normal and shear stress can be calculated for static conditions. All possible orientations of failure planes with a resolution of 5° were analysed to determine the lowest fluid pressure required to trigger failure under static conditions. The in situ stresses were calculated as a function of depth using the functions described above.

The results of the evaluation are presented in Table 5 for the "Worst Case" (Table 3) parameters for the Primary Seal, the "Reasonable Case" (Table 3) parameters for the Primary Seal and the "Fault Present" for the Secondary Seal, assuming no cohesion and only an angle of friction. These are cases

1, 2 and 3 respectively listed in Table 5. Values where the factor of safety is less than 1 are not recorded as these are scenarios which are not physically possible.

The first column in Table 5 represents depth below mean sea level, the following three columns are the fluid pressure, horizontal stress and vertical stress derived from the functions given above. Three cases 1, 2, and 3 are then presented, with the rock mechanical parameters listed at the top of each case. “Rest Safety Ratio” refers to the factor of safety under natural static conditions, i.e. no injection of fluid. “Overpressure at failure” refers to the amount of fluid pressure which can be sustained in a local, static, not regional sense. This might be understood as a pulse injection, not influencing the horizontal stress field. The static analytical modelling results are compared with dynamic numerical modelling results in Tier 4: Numerical model. “FP:SH at failure ratio” indicates the ratio of the fluid pressure to the horizontal stress when the “Overpressure at failure” is applied.

The results indicate that the parameter set representing the “Case 1: Worst Case” is not valid under static conditions as the primary seal would not be able to withstand this stress at levels down to 2600 metres under natural conditions. As this stress condition can be measured in the field, this is an indication that the mechanical parameters must be more resilient, i.e. closer to the “Case 2: Reasonable Case” parameters.

Examination of the Case 2 results indicates that failure with these rock mechanical parameters is due to the horizontal stress being exceeded, i.e. tensile failure where the total fluid pressure exceeds the total horizontal stress, and not fracturing or shear failure. Case 3 represents the pre-existing faults within the strata with no cohesion. It is interesting to note that the evaluation suggests that down to about 1700 metres the rest safety factor is minimal, suggesting that the stress distribution at this level is controlled by the presence of faulting. Failure within these strata can be triggered by a fairly low fluid overpressure. This depth is approximately the depth of the Passive Overburden and Secondary Seal contact. The secondary seal correlates with the stronger chalk group, and an increase in rate of positive increase in horizontal stress with depth.

The stability profile has been evaluated for the data on the stress profiles taken in the vicinity of the Goldeneye Gas Field (Shell, 2011a). The change in horizontal stress profile occurs at around the commencement of the Chalk Group. This is most likely due to stress bridging by the mechanically more resilient Chalk Group in the profile. It is probable that the stress profile is dependent on the depth of the Chalk Group which would suggest that where the Chalk Group exists at shallow levels, more stability can be expected due to larger horizontal stress than predicted by the evaluation presented here.

Table 5 Fluid pressure and safety limit for three different mechanical failure criteria.

				Case 1	C=0 MPa	$\phi = 13°$	Case 2	C=6 MPa	$\phi = 13°$	Case 3	C=0 MPa	$\phi = 28°$
Depth m	Fluid Pressure MPa	Horizontal Stress MPa	Vertical Stress MPa	Rest Safety Ratio	Overpressure at Failure MPa	FP:SH at Failure Ratio	Rest Safety Ratio	Overpressure at Failure MPa	FP:SH at Failure Ratio	Rest Safety Ratio	Overpressure at Failure MPa	FP:SH at Failure Ratio
1000	10.1	14.16	20.85				1.40	4.06	1.00	1.03	0.29	0.73
1200	12.1	17.14	25.32				1.42	5.04	1.00	1.04	0.43	0.73
1400	14.1	20.15	29.87				1.43	6.05	1.00	1.04	0.57	0.73
1600	16.1	23.18	34.49				1.44	7.08	1.00	1.04	0.70	0.72
1800	18.1	26.23	39.18				1.45	8.13	1.00	1.05	0.82	0.72
2000	20.1	30.70	43.95				1.53	10.59	1.00	1.16	3.12	0.76
2200	22.1	35.50	48.78				1.61	13.40	1.00	1.27	5.90	0.79
2400	24.1	40.54	53.69				1.68	16.44	1.00	1.37	9.01	0.82
2600	26.1	45.80	58.67				1.75	19.70	1.00	1.48	12.44	0.84
2800	28.1	51.28	63.72	1.06	1.79	0.58	1.83	23.18	1.00	1.58	16.16	0.86
3000	30.1	56.97	68.85	1.21	6.45	0.64	1.89	26.87	1.00	1.67	20.17	0.88
3200	32.1	62.87	74.05	1.36	11.55	0.69	1.96	30.77	1.00	1.76	24.46	0.90
3400	34.1	68.96	79.31	1.50	17.05	0.74	2.02	34.86	1.00	1.85	29.02	0.92
3600	36.1	75.24	84.66	1.64	22.95	0.78	2.08	39.14	1.00	1.94	33.83	0.93
3800	38.1	81.71	90.07	1.77	29.24	0.82	2.14	43.61	1.00	2.02	38.89	0.94
4000	40.1	88.36	95.55	1.90	35.89	0.86	2.20	48.26	1.00	2.10	44.20	0.95
4200	42.1	95.19	101.11	2.02	42.91	0.89	2.26	53.09	1.00	2.18	49.75	0.96
4400	44.1	102.19	106.74	2.14	50.26	0.92	2.32	58.09	1.00	2.26	55.52	0.97

Explanation of terms

Depth — Depth in metres below mean sea level at which the stability is analysed
Fluid Pressure — Natural fluid pressure at depth given
Horizontal Stress — Horizontal stress at given depth
Vertical Stress — Vertical stress at given depth
Rest Safety Ratio — Factor of safety equation (6) with no fluid injection at this depth for these mechanical parameters
Overpressure at Failure — Amount of extra fluid pressure at this depth likely to cause failure
FP:SH at Failure Ratio — Total fluid pressure to horizontal stress ratio at this depth at failure. A value of 1 indicates tensile failure

Tier 3: An empirical function to summarise the static geomechanical results

To enable the geomechanical results to be portable to other codes and usable for the whole of the Captain Sandstone Fairway, empirical multivariate functions were derived which allowed the maximum possible overpressure to be retained by the Primary Seal, the Secondary Seal or Faults to be expressed as a function of depth. It should be noted that this is for the static geomechanical conditions, that is dynamic regional changes to the horizontal stress as a result of fluid pressure increase is not taken into account. These are accounted for in Tier 4.

For the Primary Seal the maximum overpressure is given by (21) valid from 1000 metres to 4500 metres depth.

$$P_{f\_static} = \frac{a}{\left[1+\left(\frac{z}{b}\right)^{c}\right]^{d}} \qquad \begin{aligned} a &= 100 \\ b &= 5601.22 \\ c &= -8.17113 \\ d &= 0.258517 \\ z &= \text{ depth in (m)} \\ P_f &= \text{ failure overpressure in MPa} \end{aligned} \qquad \textbf{(21)}$$

For the Secondary Seal and Faults the maximum overpressure is given by (22), valid from 1000 meters to 4500 metres depth.

$$P_{f\_static} = e^{\left(a+\frac{b}{z}\right)+(c\ln z)} \qquad \begin{aligned} a &= 9.77318 \\ b &= -11011.5 \\ c &= -0.3883 \\ z &= \text{ depth in (m)} \\ P_f &= \text{ failure overpressure in MPa} \end{aligned} \qquad \textbf{(22)}$$

The modelling results presented in Table 5 are illustrated for the primary seal and the secondary seal in Figure 6, as is the fitting using the empirical formulas given above. This figure also includes the results of the Tier 4 modelling where the dynamic effect of regional fluid pressure increase is taken into account.

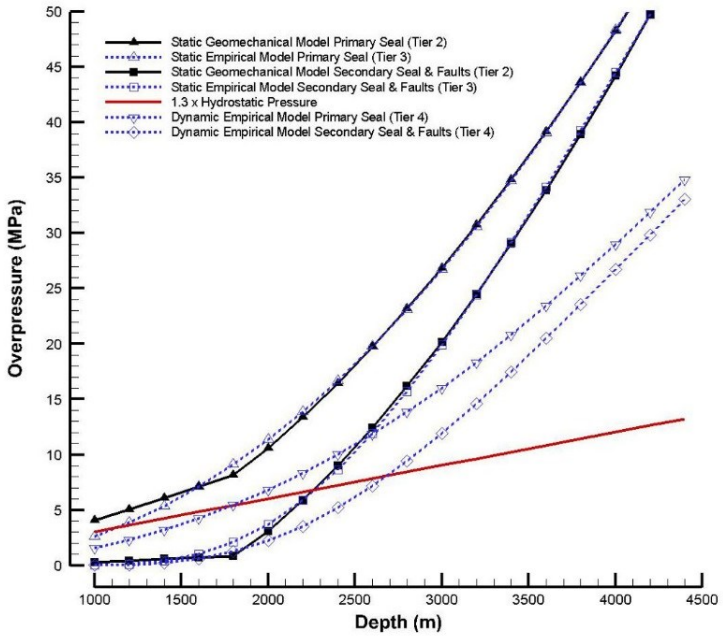

Figure 6 Primary Seal, Secondary Seal and Fault Overpressure Limits: Comparison of static stress (Tier 2), empirical fitting (Tier 3) and dynamic stress (Tier 4) results as well as a simple hydrostatic pressure stress limit assumption.

Tier 4: Numerical modelling of dynamic stress conditions

Numerical models are able to take into account heterogeneity in the analysis of the problem to be solved. Although several simplifications have to be made, the numerical models come closer to reality than analytical approaches. The numerical analysis performed involved the solution of the Thermal, Hydraulic and Mechanical balance equations. The open source coupled process simulator OpenGeoSys (OGS) was used to solve the coupled process problems. The theory and several benchmarks regarding the use of OGS may be found in Kolditz et al. (2012). The following provides an overview of the multi-physics problems solved.

Following Lewis and Schrefler (1998) the momentum balance equation can be written as

$$L^T \boldsymbol{\sigma} + \rho \mathbf{g} = o \qquad \textbf{(23)}$$

For a single solid phase, ρ is the solid density (kg/m^3), $\mathbf{g}$ is the acceleration due to gravity (m/s^2). The differential operator L is defined as

$$L = \begin{bmatrix} \frac{\partial}{\partial x} & 0 & 0 \\ 0 & \frac{\partial}{\partial y} & 0 \\ 0 & 0 & \frac{\partial}{\partial z} \\ \frac{\partial}{\partial y} & \frac{\partial}{\partial x} & 0 \\ 0 & \frac{\partial}{\partial z} & \frac{\partial}{\partial y} \\ \frac{\partial}{\partial z} & 0 & \frac{\partial}{\partial x} \end{bmatrix} \quad \textbf{(24)}$$

The stress tensor represented as a vector such that

$$\boldsymbol{\sigma} = \begin{Bmatrix} \sigma_x & \sigma_y & \sigma_z & \tau_{xy} & \tau_{yz} & \tau_{xz} \end{Bmatrix}^T \quad \textbf{(25)}$$

The strain is given as

$$\boldsymbol{\varepsilon} = \begin{Bmatrix} \varepsilon_x & \varepsilon_y & \varepsilon_z & \gamma_{xy} & \gamma_{yz} & \gamma_{xz} \end{Bmatrix}^T \quad \textbf{(26)}$$

The constitutive relationship of strain to stress is given as

$$d\boldsymbol{\sigma} = \mathbf{D} d\boldsymbol{\varepsilon} \quad \textbf{(27)}$$

Strain is related to displacement $\mathbf{u}$

$$d\boldsymbol{\varepsilon} = L d\mathbf{u} \quad \textbf{(28)}$$

This is solved as a boundary value problem where $\mathbf{u} = \mathbf{u}_0 \ \text{in } \Omega \text{ and on } \Gamma \quad \mathbf{I}^T\boldsymbol{\sigma} = \mathbf{t}$

Where $\mathbf{I}$ is related to the unit normal vector $\mathbf{n} = \begin{Bmatrix} n_x & n_y & n_z \end{Bmatrix}^T$ by

$$\mathbf{I} = \begin{bmatrix} n_x & 0 & 0 \\ 0 & n_y & 0 \\ 0 & 0 & n_z \\ n_y & n_x & 0 \\ 0 & n_z & n_y \\ n_z & 0 & n_x \end{bmatrix} \quad \textbf{(29)}$$

For evaluation of coupled flow in a saturated porous medium we require the mass balance equation for fluid flow

$$Ss \frac{\partial p_w}{\partial t} + div\left[\frac{k}{\mu^w} \left(-\text{grad}\, p_w + \rho_w \mathbf{g} \right) \right] = 0 \quad \textbf{(30)}$$

Where Ss is the specific storage of the porous media, described above in (16), k is the permeability in (m^2), μ^w is the viscosity of the fluid in (Pa.s^{-1}), p_w is the fluid pressure in (Pa). Coupling of the

fluid flow and momentum balance equations is accomplished by considering effective stress such that

$$\boldsymbol{\sigma}' = \boldsymbol{\sigma} - \alpha_b \mathbf{m} p_w \tag{31}$$

Where α_b is the Biot Willis coefficient, $\boldsymbol{\sigma}'$ is now considered to be the effective stress and

$$\mathbf{m} = \begin{bmatrix} 1 & 1 & 1 & 0 & 0 & 0 \end{bmatrix}^T \tag{32}$$

Strictly speaking the Biot Willis coefficient should also be evaluated in the calculation of the storage coefficient. As a first approximation during modeling this coefficient was set at 1, meaning there is a full transfer of fluid pressure to the rock skeletal stress, thereby making the formulation used for the specific storage in (16) valid.

The solution of (30) provides the fluid pressure distribution throughout the modelled area. This can be used to derive the fluid velocity v which can then be used to solve the advective heat transport equation given in (33)

$$c\rho \frac{\partial T}{\partial t} + c^w \rho^w v \cdot \nabla T - D\nabla^2 T = \rho Q_T \tag{33}$$

where c is the specific heat capacity of the saturated porous rock (J/kg.K), c^w is the specific heat capacity of the fluid, D is the heat diffusion dispersion tensor for the porous medium, T is temperature, ρ^w is fluid density, ρ is density of the saturated porous rock, and Q_T is the heat source or sink. Here, after De Marsily (1986), the heat diffusion dispersion tensor contains a component for pure diffusion and a component for dispersion due to advection, i.e.:

$$D_\alpha = \lambda_m + v_\alpha \beta_\alpha \tag{34}$$

where D_α is the heat diffusion dispersion coefficient in the α -direction (J/Kms), λ_m is the isotropic heat conductivity of the porous medium (J/Kms), v_α is advective flow velocity in the α -direction, and β_α is the heat dispersion coefficient in the α -direction. The value β_α is the product of the directional (longitudinal or transverse) dispersion coefficient, with $c^w \rho^w$.

The inclusion of thermal stress in the evaluation is such that

$$\Delta\varepsilon = D\left(\Delta\varepsilon^e - \alpha_t \Delta T\right) \tag{35}$$

where α_t is the thermal expansion coefficient. A staggered finite element solution procedure was applied to evaluate the above equations, with the order Hydraulics, Thermal, Mechanical. A more detailed description of the finite element method can be found in works such as Lewis and Schrefler (1998) and Zienkiewicz and Taylor (2005).

Models and Meshes

The aim of the modelling was to investigate in as much detail as possible the THM geomechanical response of the Captain Sandstone Fairway during injection of dense phase CO_2 at multiple sites. The results of the THM modelling were then used to augment the Tier 3 empirical model, and account for dynamic stress. Computationally it was not possible to model the whole of the ~1300 km^2 area at high resolution. Therefore models were constructed in 2D and 3D to enable key engineering relevant parameters to be determined and the impact of coupled processes to be investigated at sufficient

resolution. These models, with their main features and purposes are listed in Table 6, and described in more detail below.

To model the thermal pulse and the development of thermal stress in the vicinity of the injection well, a mesh resolution significantly lower than the thickness of the geomechanical facies layers affected was necessary. 2D cross sections using both quad and triangular elements with a mesh resolution of ten metres in the reservoir and base of the primary seal were generated (Figure 7**,** Figure 8 and Figure 9). The section dimensions were of the order of up to 3 km depth X 6 km width. The geometry of the sections was asymmetrical hence an axisymmetric simulation was not possible.

To investigate the approximate magnitude of the expected fluid pressure increase in the storage complex for the given injection rates, a 3D regional geomechanical model of the Captain Sandstone Fairway was created with mesh dimensions of the order of 130 km length, 10 km width and 4 km depth using non regular hexahedral elements. The mesh resolution was selected to be 50 metres in the vicinity of the injection wells at Site A and Site B (Figure 10).

Table 6 List of models and meshes, main features and purposes

Model and key feature	Main purpose
3D Regional model 130 km x 10 km x 4 km, non-regular hexahedral elements, mesh resolution was selected to be 50 metres in the vicinity of the injection wells	Determine the magnitude of the fluid pressure increases in the reservoir expected as a result of the injection rates. Source terms in the 2D models (following) were set accordingly to generate the same fluid pressure
2D Generic cross section, where the reservoir is at a depth of 3000 m, mesh resolution down to 10 m.	Investigation of the impact of the coupling and main controls of the THM processes on fluid pressure, stress and thermal stress distribution in the storage complex.
2D Cross section at injection site A, mesh resolution down to 10 m.	Evaluation of the THM geomechanical stability in detail at site A
2D Cross section at injection site B, mesh resolution down to 10 m	Evaluation of the THM geomechanical stability in detail at site B

Due to the size of the meshes generated a number of calculations were performed using the parallel capability of OpenGeoSys on eight cores.

The meshes were generated using Gmsh, (Geuzaine and Remacle 2009), geometry selected from data provided derived in this study and from Shell (2011a,b,c). The injection pressures predicted in the 3D geological model at the locations of Site A and Site B were used to inform the rate of injection in the 2D sections to match the anticipated overpressures. The injection rates in the 2D models were chosen such that the maximum pressure predicted in the 3D models was slightly exceeded to allow a further degree of safety.

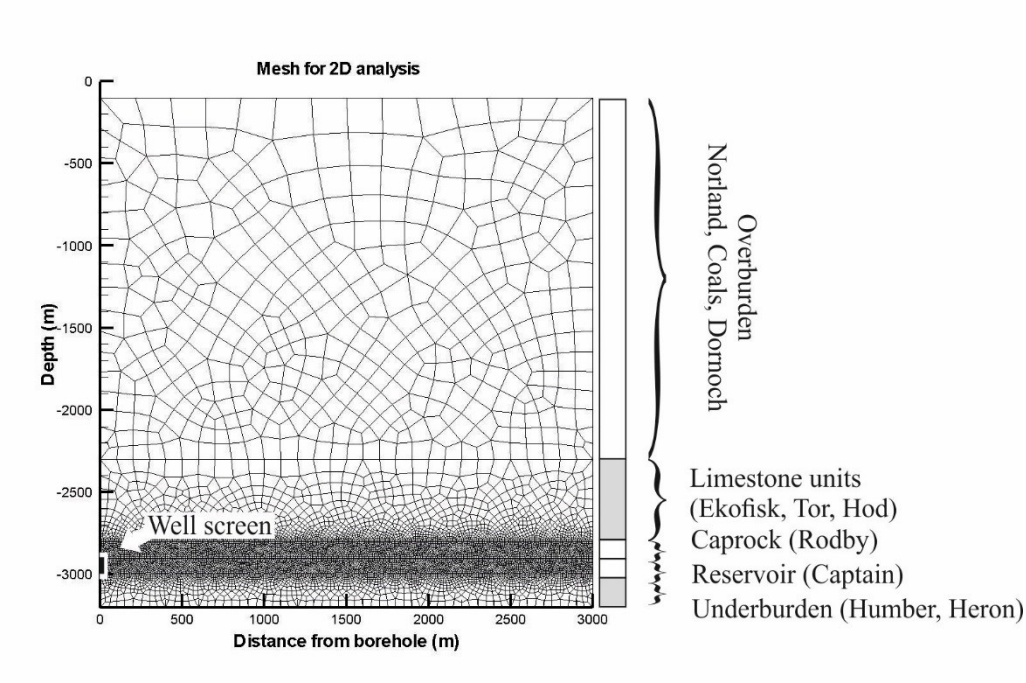

111

112 **Figure 7 Mesh used for 2D analysis of a general cross section for the Captain Sandstone Fairway**

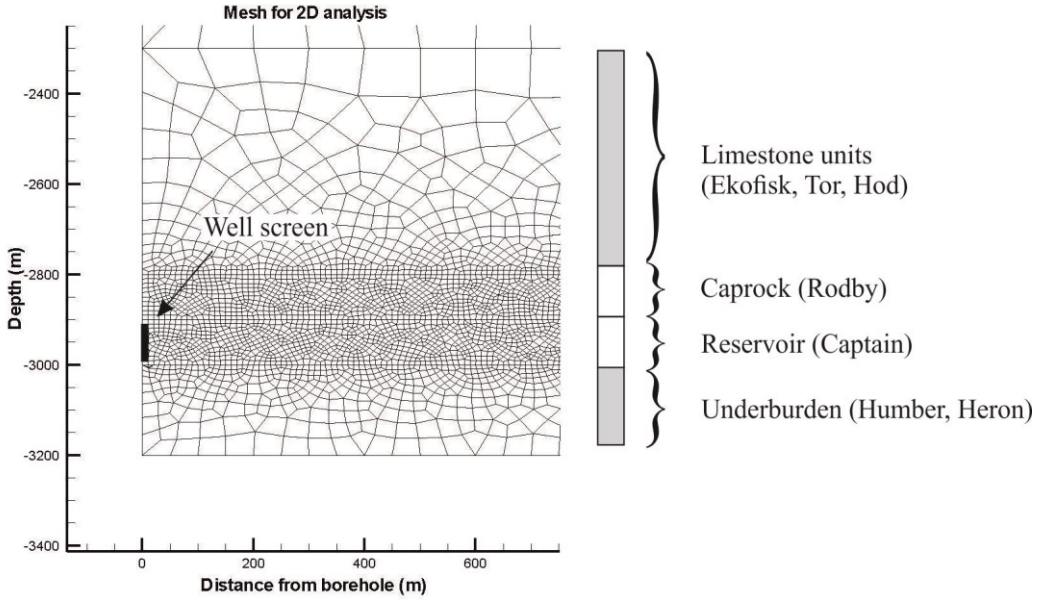

113

114 **Figure 8 Close up view of mesh used for 2D analysis of a general cross sections for the Captain Sandstone fairway**

115

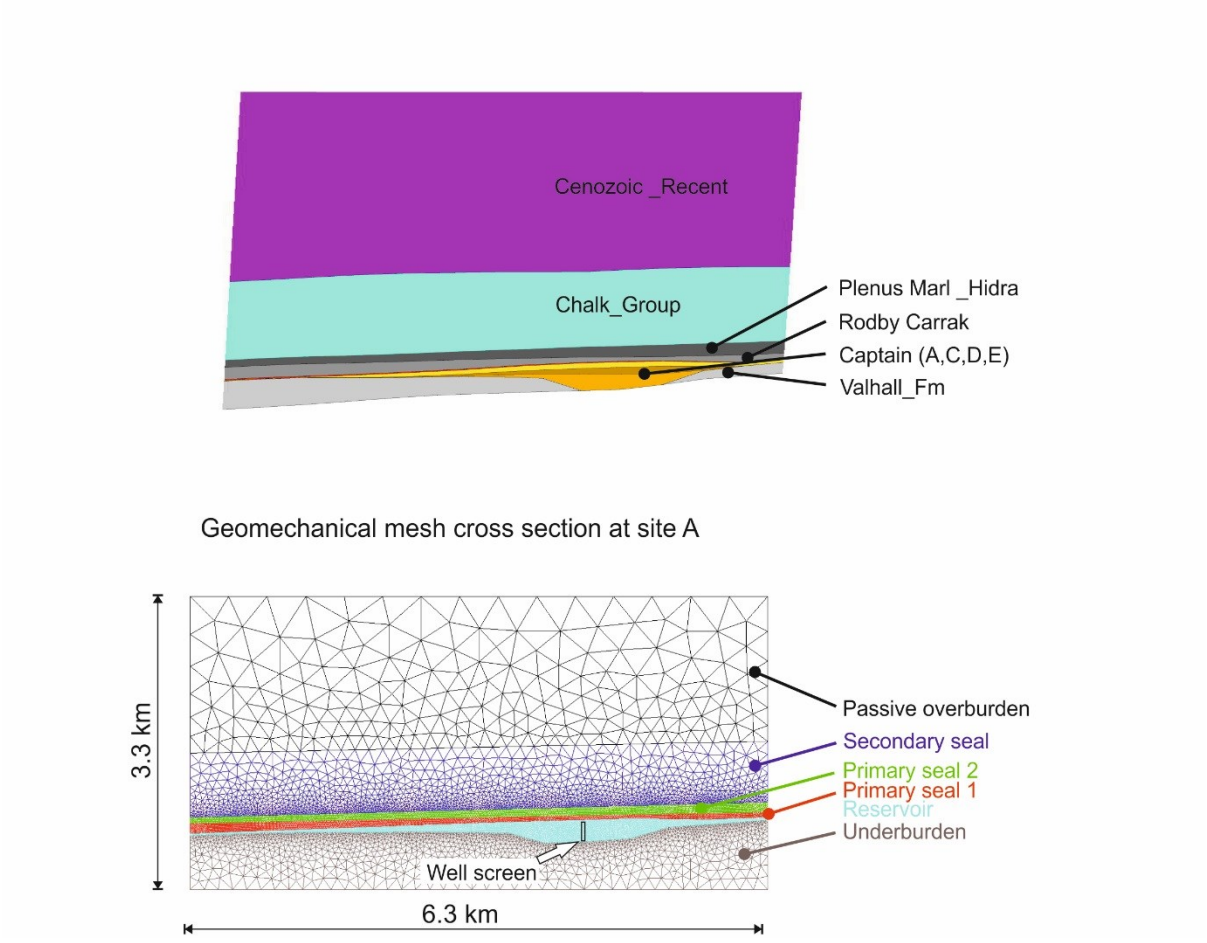

Figure 9 Cross section of Captain Sandstone Fairway at injection site A, mesh and geometry for detailed THM modelling

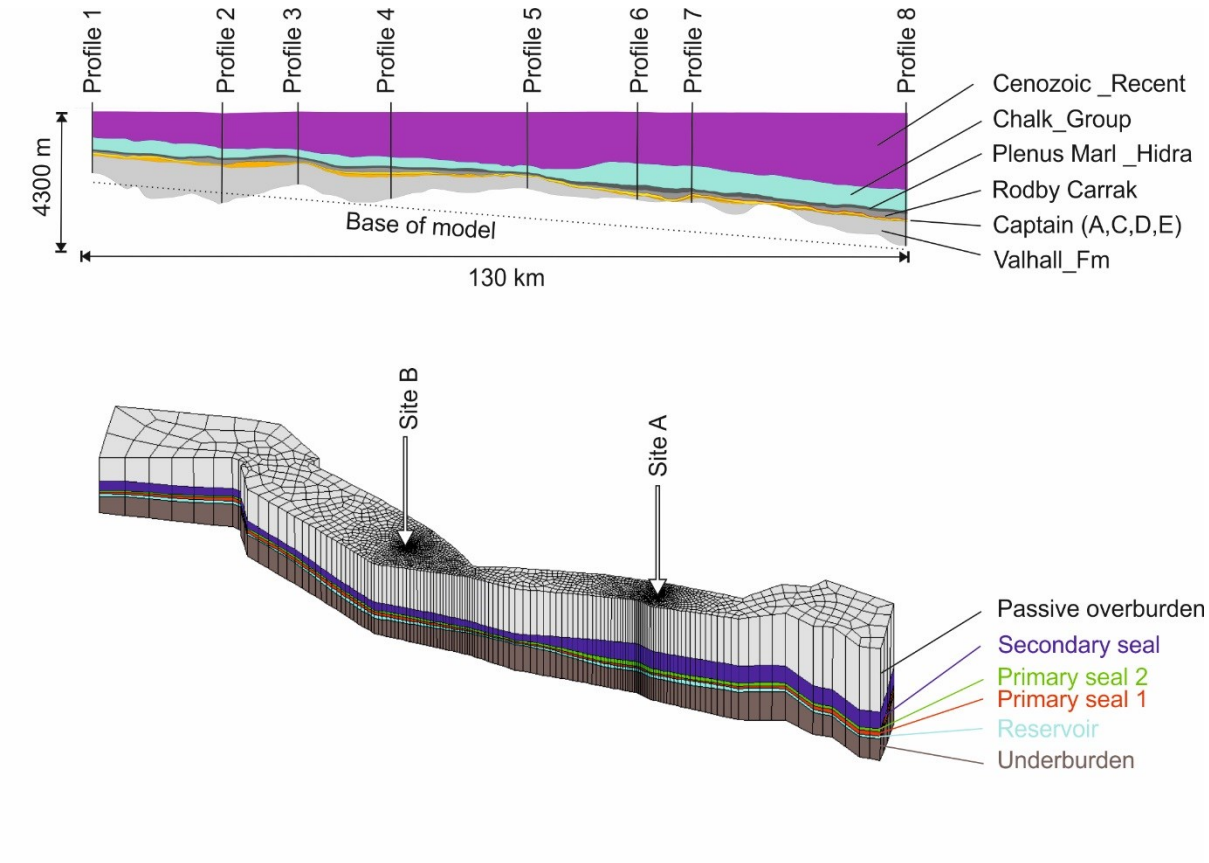

Figure 10 3D mesh of the Captain Sandstone Fairway used for the evaluation of the fluid pressure response during injection of dense phase CO_2.

Numerical Model Validation

Both the fluid pressure predictions and the deformation predictions of the numerical model were validated against other modelling approaches and previous work.

Parallel to the development of the geomechanical model presented here, Eclipse was used to simulate a discrete multiphase model of the Captain Sandstone Fairway for a single statistical realisation of the Captain Sandstone Fairway. This model assumed that base of the reservoir facies was closed to fluid flow. The pressure connectivity predicted between sites A and B was shown to be very similar to the connectivity predicted by the geomechanical model with similar boundary conditions.

Shell (2011a) present a 3D model of the Goldeneye Gas field whereby they investigate the surface deformation as a result of gas extraction from the Goldeneye field. They present modelling results for a reservoir under pressure of circa 10 MPa. They obtain a surface deformation of 4.6 cm subsidence of the sea floor, with the deformation extending 14 km east-to-west and 9 km north-to-south. Using the current model for the Captain Sandstone Fairway (3D model and different geometry), with the parameterisation presented in Table 3 (injection parameters rather than extraction parameters) the sea floor subsidence predicted by this model is 3 cm for the sea floor and the extent is similar to the Shell (2011a) model. There is no specification of the limit of deformation, e.g. 1 mm or less, so only an estimate of the extent can be made here.

Additionally the OpenGeoSys code is extensively documented with respect to comparison against benchmarks (Kolditz and Shao 2012). Therefore it can be taken that the model is reasonably well validated.

Modelling Results

Reservoir overpressure limit and impact of thermal stress

Both 2D and 3D geomechanical modelling results are presented. First selected results are presented for a generic 2D cross section in the Captain Sandstone Fairway, where the Reservoir is found at a depth of circa 3000 metres.

1. A fluid overpressure of 2.2 MPa at the injection well, after 30 years of injection at realistic commercial injection rates in a generic cross section (Figure 11).
2. A fluid overpressure of 2.2 MPa and a temperature of 20°C, that is about 60°C below the reservoir temperature, after 30 years of injection at a realistic commercial injection rate in a generic cross section close to Site A.

The factor of safety prior to any injection in the vicinity of the well is presented in Figure 12. The effect of considering only the fluid pressure in the calculation of the factor of safety for 2.2 MPa injection overpressure is presented in Figure 13. The thermal impact of the injection of $scCO_2$ after 30 years is presented in Figure 14, and the case where both the fluid pressure and the thermal stress is considered is presented in Figure 15.

To understand the impact of including the thermal stress, the change in the factor of safety from the fluid only case to the fluid and thermal case is presented in Figure 16. The change in the factor of safety can be directly related to the change in the horizontal stress field (Figure 17). As the Reservoir contracts due to the thermal stress, the horizontal stress component is carried by stress-bridging through the stiffer layers of the Chalk Group and the Underburden. The factor of safety of the Chalk Group acting as the secondary seal increases slightly as a result of this effect. The Primary Seal, because it is not so stiff accommodated the change in stress through more strain. Additionally the stress field itself is rotated, Figure 18.

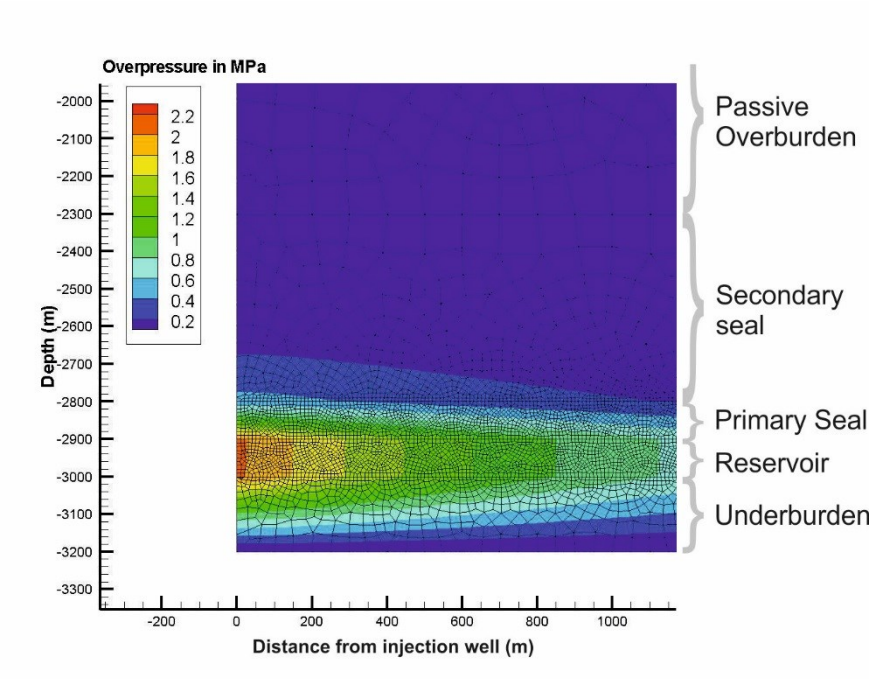

Figure 11 Fluid overpressure in MPa after 30 years of injection in the 2D general model scenario, well screen bottom left, ~2900 m to 3000 m.

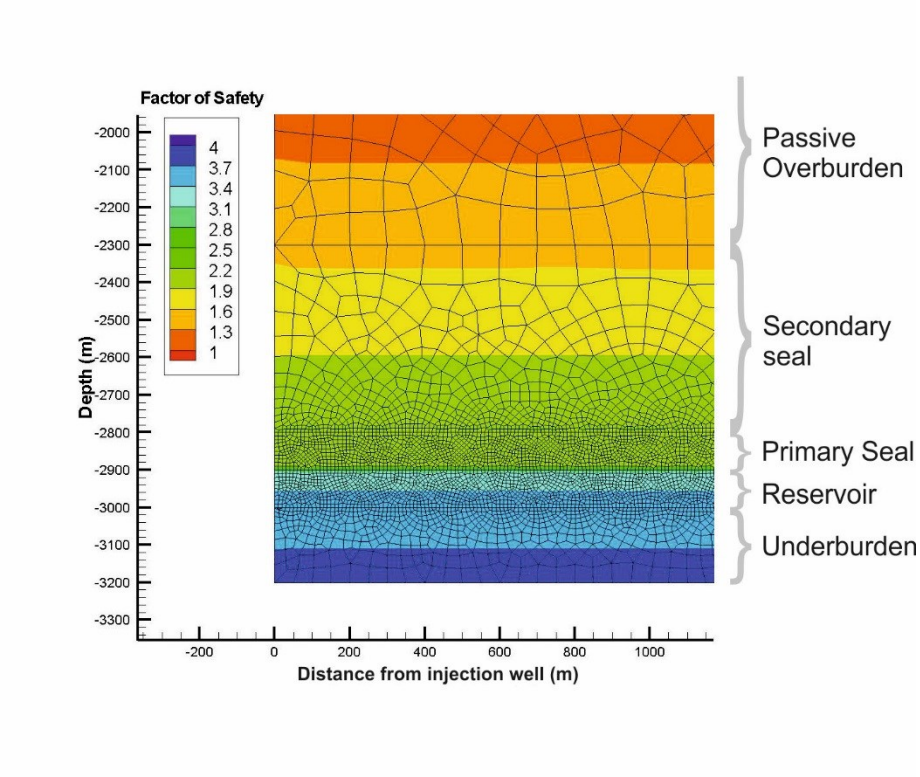

169

170 **Figure 12 Initial factor of safety without fluid injection**

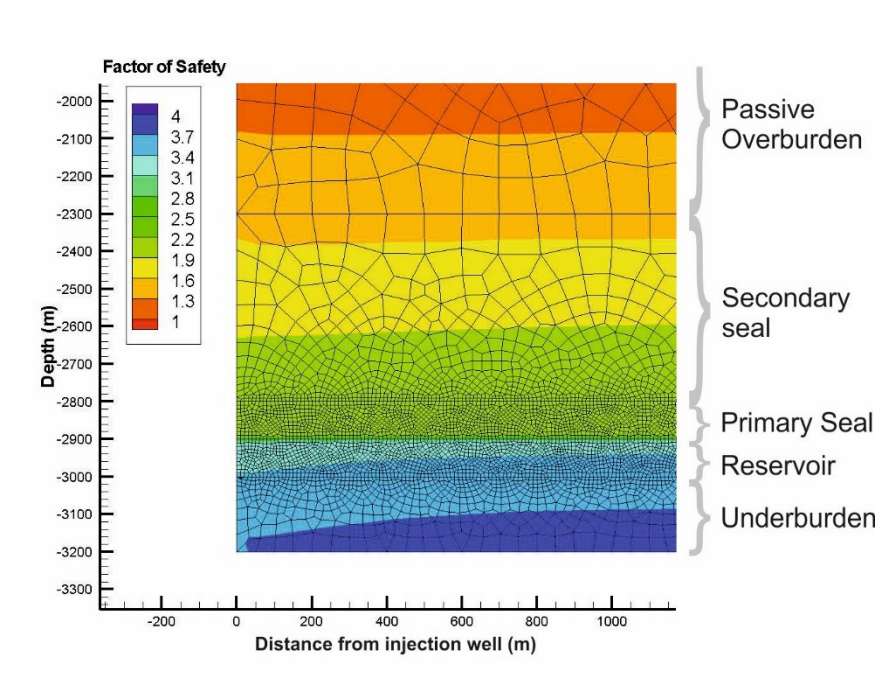

171

172 **Figure 13 Factor of safety for 2.2 MPa overpressure, for fluid injection without thermal stress, well screen bottom left,**
173 **~2900 m to 3000 m.**

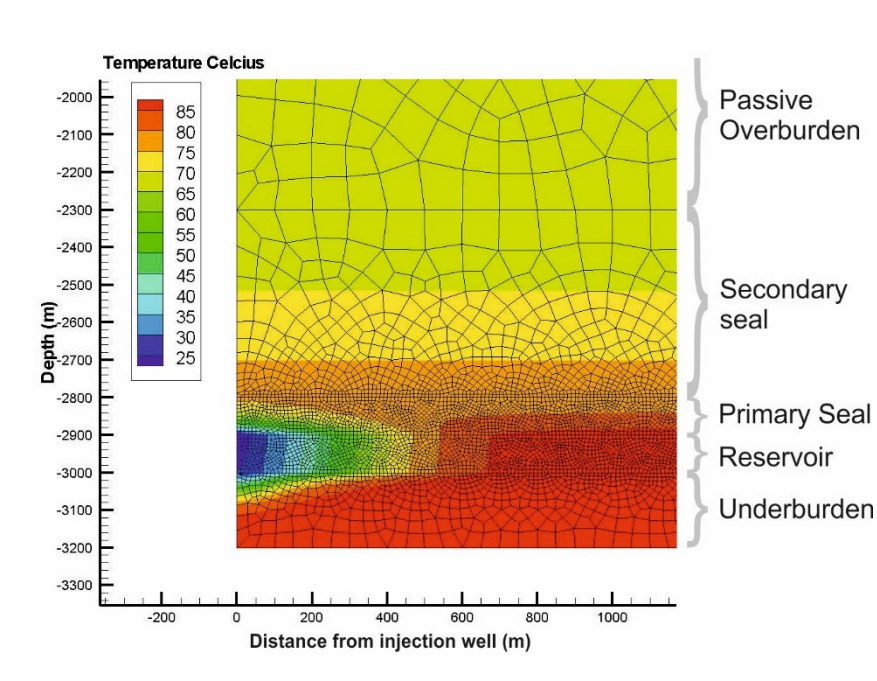

Figure 14 Temperature profile after 30 years of injection in the 2D general model scenario, well screen bottom left, ~2900 m to 3000 m (SCCS 2015).

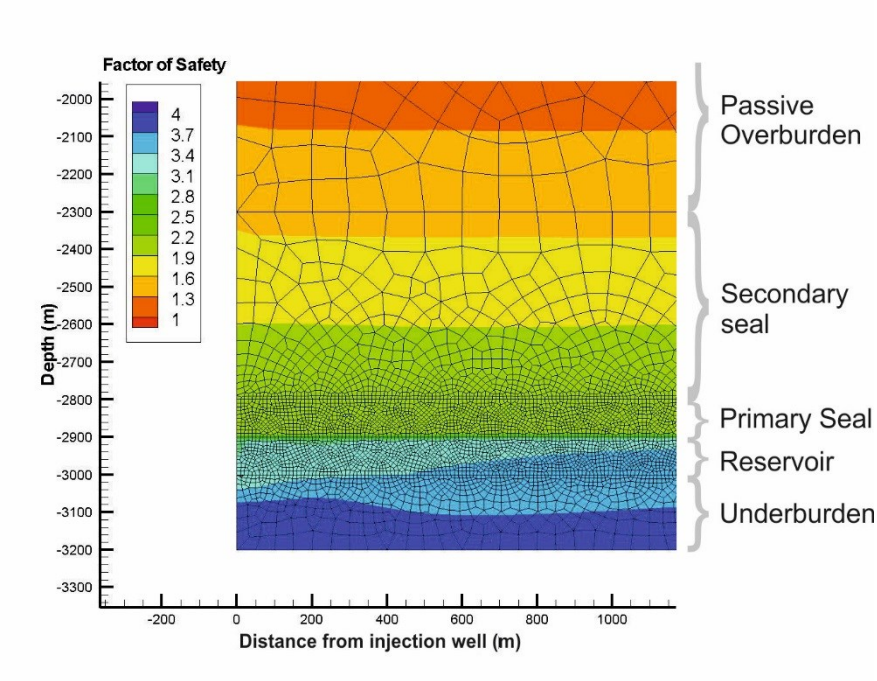

Figure 15 Factor of safety for 2.2 MPa overpressure, for fluid injection with thermal stress, well screen bottom left, ~2900 m to 3000 m.

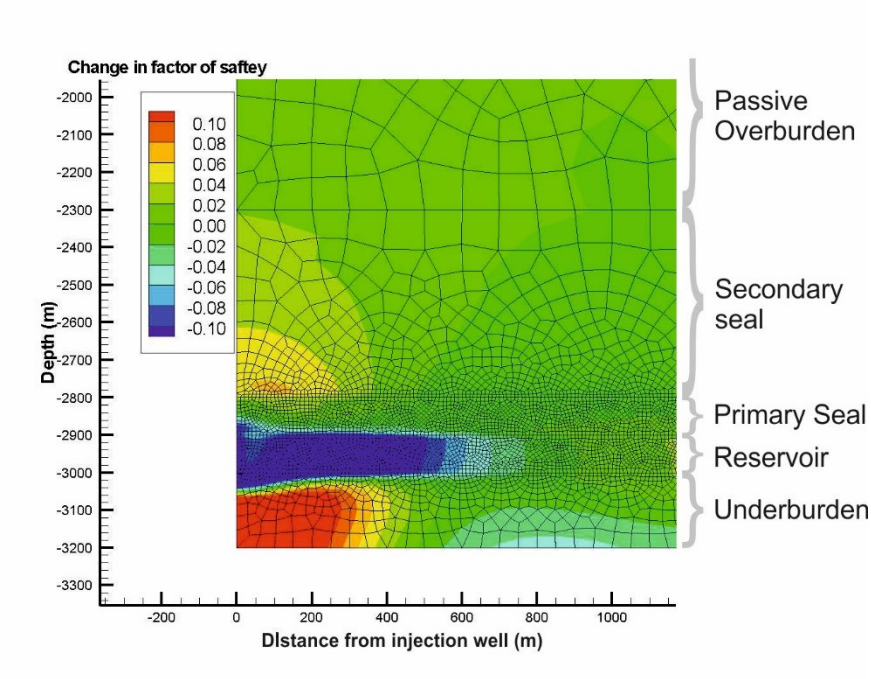

Figure 16 Change in factor of safety as a result of thermal stress. Positive values (pale green to red) indicate an increase in the safety factor, well screen bottom left, ~2900 m to 3000 m.

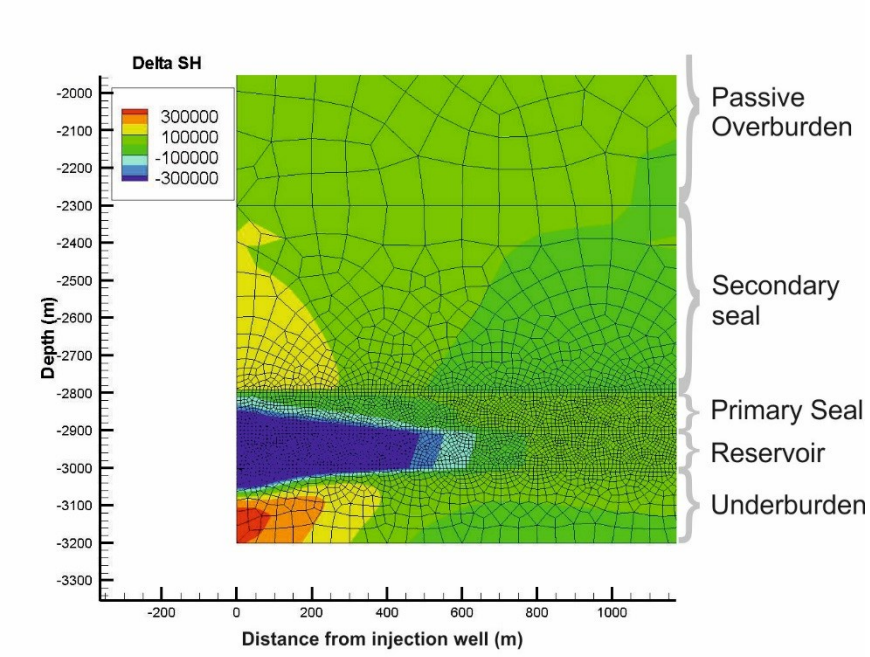

Figure 17 Change in horizontal stress field due to the impact of thermal stress, well screen bottom left, ~2900 m to 3000 m.

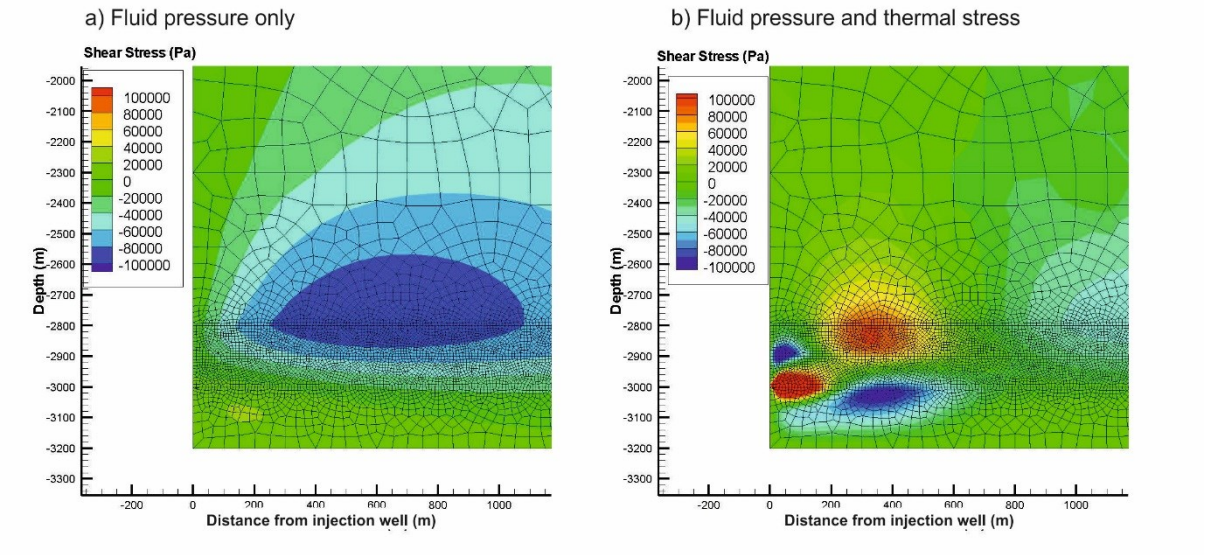

Figure 18 Rotation of stress field a) caused solely by fluid injection and b) caused by fluid injection thermal stress, well screen bottom left, ~2900 m to 3000 m (SCCS 2015).

The above figures (Figure 12 to Figure 18) illustrate the generic response of the Reservoir to the injection of $scCO_2$. The stress redistribution is a function of the nature of the interaction of the geomechanical facies, their mechanical properties and their hydraulic properties.

Different strata exhibit several different orders of magnitude difference in terms of their permeability. The location of the fluid pressure changes are controlled by the heterogeneity between the layers in their permeability. The main fluid pressure change is seen in the reservoir facies, and contained in the reservoir by the overlying and underlying strata.

In contrast the mechanical properties of the different strata are within an order of magnitude of one another, and so the stress distribution is more wide spread. Stiffer layers carry more of the stress loading than the softer layers and so are more effected than the softer layers by any increases or decreases in the stress field. Hence the stress distribution follows the general trend of the strata in terms of geometry, but this is not so pronounced as the fluid flow.

It can be seen from the equation (33) that the thermal pulse is controlled by a diffusive and advective term. The diffusive thermal parameters are all of a similar magnitude. This means that the diffusive thermal signal is spherical. However the advective thermal signal is controlled by fluid flow and therefore directly related to the permeability distribution of the system.

The overprint of the thermal stress changes and the fluid stress changes on the regional stress leads to a slight enhancement of the stability of the secondary seal. The reason for this is illustrated in Figure 17. As the area around the injection well within the reservoir cools, so the reservoir contracts and carries less of the regional horizontal stress meaning that the stronger overlying and underlying strata carry more stress. These results are specific to this sequence of strata and the contrast in mechanical and hydraulic parameters of the modelled layers.

Fjaer et al. 2008 showed that for a rigidly constrained plate in the horizontal plane that the longer term change in horizontal stress due to thermal stress changes around the borehole is given by the analytical expression

$$\Delta S_h = \frac{E}{(1-v)} \alpha_t \Delta T \qquad \textbf{(36)}$$

This is an analytical model assuming fully ridged boundary conditions allowing. In this unrealistic case it would suggest a value of up to 9 MPa change in horizontal stress for the reservoir strata and circa 5 MPa for the primary seal for a 60 C drop in temperature. In reality the strata is not restrained horizontally or vertically, so the strain from the thermal stress is accommodated over a large area. The numerical model suggests that the maximum change in horizontal stress due to the thermal stress is of the order of 0.3 MPa. The numerical model has not taken into account possible very near borehole effects, cementing features and potential very local stress bridging. However the thermal stress superimposes on the regional horizontal stress, which is of the order of 30 MPa. Any impact of thermal stress within the strata of the Captain Sandstone Fairway is most likely to be localized, minimal and of a consolidation nature.

Significance of the basal boundary (connectivity and surface deformation)

During hydrocarbon production the nature of the basal boundary is usually of secondary importance. However, when considering the regional pressure increase during fluid injection into a reservoir, the nature of the underburden becomes highly significant. Fluid pressure in the reservoir can be dissipated either through lateral connection to other strata, or vertically. The areal extent of the connection of the underburden with the reservoir is extremely large, therefore even a low permeability Underburden enables significant fluid flow and therefore makes pressure dissipation through the Underburden very significant. The pressure connectivity between Site A and Site B is negligible for the case where the basal boundary is open to flow but the Underburden has a thickness of circa 800 metres.

For the case where the basal boundary is not open to flow the pressure connection is significant, leading to a clear connectivity between the sites. Figure 19 demonstrates this, Site A and Site B can be shown to have of 0.9 MPa pressure influence on each other after 15 years of injection.

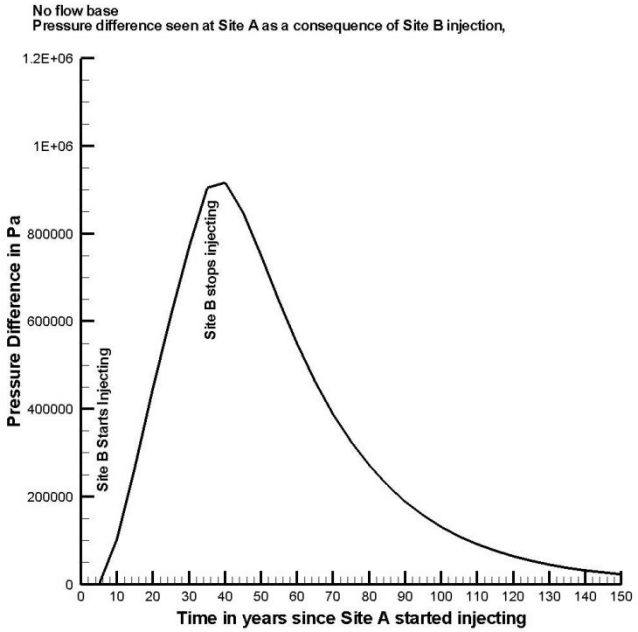

Figure 19 Pressure connection between Site A and Site B, where model basal boundary is closed to flow. Pressure difference in Pa.

Where the basal flow boundary is considered closed to flow, the fluid pressure in the reservoir is greater, and the largest amount of surface deformation is predicted, Figure 20. It is highly significant

that the vertical displacement in the positive direction extends below the level of the reservoir. This means that the strata within the Underburden are hydraulically connected to the reservoir and that the Underburden pore space is being used to accommodate fluid migration and increased pressure in the reservoir.

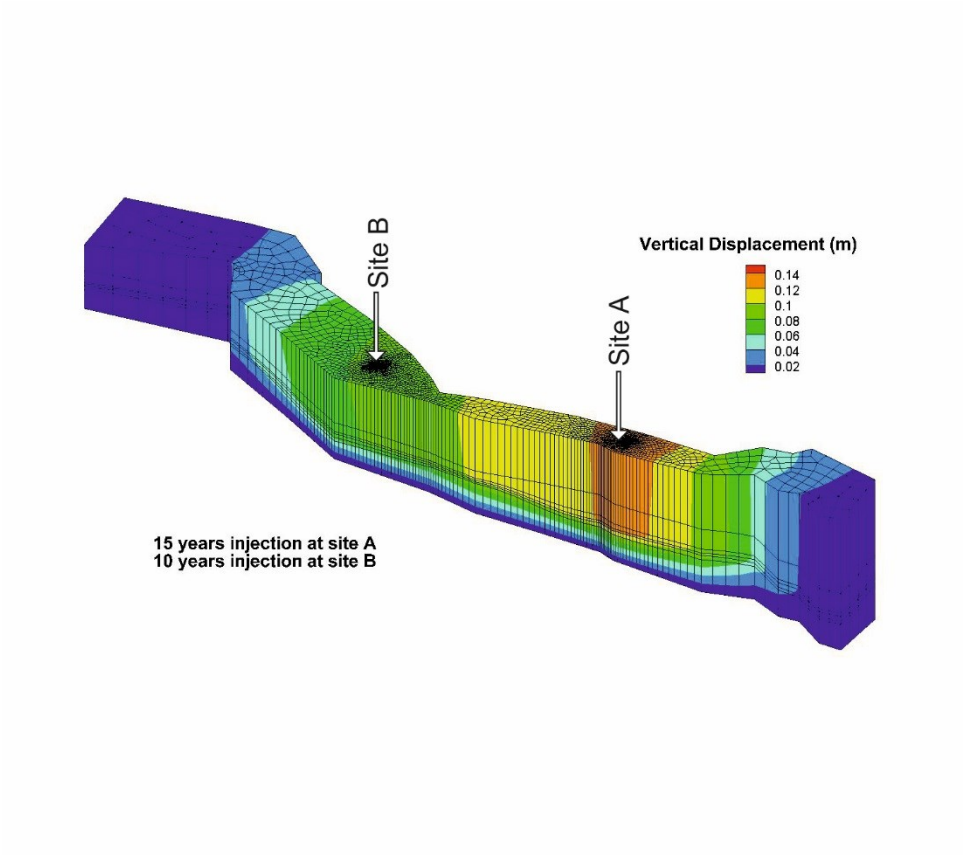

Figure 20 Deformation after 15 years CO_2 injection at Site A and 10 years injection at Site B, at an annual rate of 6 Mt/year at both sites with free surface boundary and a no-flow boundary at the base of the model

Combination of the static and dynamic geomechanical THM modelling results to provide a location dependent look up function.

In this section Tier (3) results are combined with the Tier (4) modelling to provide the final look up function to evaluate the maximum fluid pressure possible in various strata of the storage system.

The Tier (3) empirical function is based on the fitting of the analytical evaluation of the static stress conditions. Under static equilibrium conditions of stress, the vertical stress can be shown to be directly related to the horizontal stress in the strata, assuming no further tectonic stresses, where v is Poisson's ratio:

$$\sigma_H = \sigma_h = \frac{v}{1-v}\sigma_v \quad \textbf{(37)}$$

When the fluid pressure in the reservoir is increased both the vertical stress and the horizontal stress is affected. Hillis (2001) and Kim and Hosseini (2014) show that the change in horizontal stress as a result of fluid injection into a reservoir can be evaluated to

$$\Delta\sigma_H = \Delta\sigma_h = \Delta P\alpha\frac{1-2\nu}{1-\nu} \quad \textbf{(38)}$$

where α is the Biot Willis coefficient. The change in vertical stress (Kim and Hosseini 2014) can be shown to be

$$\Delta\sigma_v = \Delta P \frac{\alpha}{2} \frac{1-2\nu}{1-\nu} \quad \textbf{(39)}$$

Under static conditions the initial fluid pressure change would be under the stress conditions expressed in (37), under prolonged conditions of fluid pressure increase, where there is a regional fluid pressure change then (38) and (39) describe the dynamic stress conditions and the horizontal and vertical stress change respectively.

The relationship between the dynamic stress conditions and static stress conditions is therefore consistent throughout the storage complex, allowing a consistent relationship to be developed between the dynamic stress conditions and the static stress conditions.

For typical values of the Poisson's ratio the value of $\frac{1-2\nu}{1-\nu}$ is usually between 0.5 and 0.6. This means that for a regional fluid pressure increase there will be a partial reduction in the horizontal stress and less noticeable reduction in the vertical stress. Both of these changes impact consistently throughout the profile on the evaluation of the stability of the geomechanical facies and faults in the storage system. However this does not directly lead to a 0.5 to 0.6 reduction in the maximum predicted safe overpressure of the strata for the following reasons

- The change in fluid pressure is superimposed on the already present stress field, the change in fluid pressure may be of the order of 1-10 MPa, the existing horizontal stresses are already of the order of 20 – 40 MPa
- The analytical model assumes perfect isotropic homogeneous conditions under static stress loading. The numerical THM model accounts for the dynamic stress conditions, for the heterogeneity in the geological strata, for geometrical differences in the layers and for the impact of the thermal stress.

The Tier 4 THM modelling is used to predict the maximum overpressure the reservoir can sustain. These predications are then compared to the Tier 3 empirical predictions. Table 7 present the fluid pressure results and safety factors from the 3D and 2D models at sites A and B. The 3D model provided the predicted overpressure in the reservoir as a function of the expected injection rates in the storage asset (5.8 MPa, 6.0 MPa). These overpressures were then simulated with slight safety margin in the 2D sections (6.3 MPa, 6.6 MPa). The ratio of horizontal stress to fluid pressure and the minimum factors of safety to shear failure were then determined in the profile. In some cases the worst case values were clearly impacted by the local geometry of the layers and a small distance from the injection wells. It can be seen that at 6.6 MPa site B is just entering tensile failure. At 6.3 MPa site A is safe. In order to compare the predicted maximum possible overpressure with the Tier 3 empirical predictions it is necessary to find the overpressure at which the site A would start to fail, this is expressed under the row "Site A limit" in Table 7

Table 7 Overpressures simulated and safety margin for model with closed flow boundary at base.

	Over Pressure prediction from 3D model with closed basal flow boundary.	Over Pressure simulated in 2D model	Maximum fluid pressure to horizontal stress ratio in Reservoir // Primary Seal contact	Minimum factor of Safety in base of Primary Seal
Site A	5.8 MPa	6.3 MPa	0.78	1.64
Site A limit		11.0 MPa	0.96	1.58
Site B	6.0 MPa	6.6 MPa	0.97	1.27

The Tier (3) empirical model results (P_{f_static}) is an empirical approximation of the Tier (2) "perfect" analytical solution, and acts as a reference value against which the dynamic case with heterogeneity, geometrical variations and thermal stress influence can be compared. Table 8 presents the maximum pressure predictions of Tier (3) empirical model (P_{f_static}) and the Tier (4) THM models of the sites A and B. The ratio of the models values of P_{f_static} to the THM models are 1:0.63 and 1:0.61 respectively. From this the maximum dynamic overpressure $P_{f\_dynamic}$ for the primary seal and $P_{f\_dynamic}$ for the secondary seal and faults is given by multiplying these values of P_{f_static} from equations (21) and (22) respectively by 0.6.

$$P_{f\_dynamic} = P_{f\_static} \times 0.6 \quad \textbf{(40)}$$

Table 8 Comparison of static, THM and lookup function values for Site A and B for the primary seal

	P_{f_static}	THM dynamic model prediction	$P_{f\_dynamic}$
Site A	10.4 MPa	6.6 MPa	6.24 MPa
Site B	18.0 MPa	11.0 MPa	10.8 MPa

$P_{f\_dynamic}$ is now exported as a simple look up function which can be used to estimate the maximum overpressure possible within the storage strata under dynamic stress conditions for the primary seals, the secondary seal and the faults. The pressures predicted for key strata locations at Site A and Site B are presented in Table 9, and illustrated for the whole profile in Figure 6. Also on this figure is a commonly used simplified estimate of the maximum possible fluid overpressure presented as 1.3 x hydrostatic pressure. Whilst the hydrostatic approach provides a reasonable estimate down to about 1800 metres, below this it underestimates the amount of possible overpressure.

Table 9 Maximum injection overpressure (OP) values at injection sites after correction for thermal stress and fluid pressure for the primary seal.

	Site A		Site B	
	Depth	Max OP	Depth	Max OP
Primary Seal Base	2523 m	10.8 MPa	1912 m	6.24 MPa
Primary Seal Top	2304 m	9 MPa	1727 m	4.98 MPa
Base Secondary Seal	2304 m	4.38 MPa	1727 m	0.96 MPa
Faulting to Reservoir	2523 m	6.36 MPa	1912 m	1.8 MPa

In this case the thermal stress has been shown not to have a significant impact on the safety, and it is accommodated in the factor 0.6. However where there is a significant impact this factor can be revised in the vicinity of the boreholes. Where faulting is known to extend to the reservoir than the secondary seal and faulting values should be applied.

Discussion of the application of the four tier approach and application to other storage complexes.

The key simplification and advantage of this methodology is to be able to express all the complex geomechanical calculations including expected heterogeneity and stress superposition as an empirical multivariate expression which acts as a look up function for determining the overpressure a strata can withstand. This enables easy application by other users.

The application of the geomechanical facies concept for Tier (1) is relatively new, but covered in the literature. It provides a fundamental building bock to understanding the behavior of any storage

complex. The analytical solutions used for Tier (2) are well established and found in any rock mechanics text book. The use of a multivariate function to approximate the results of Tier (2) analysis throughout the storage complex and provide the Tier (3) approximation under static stress conditions has not been done before to the author's knowledge. Combining the Tier (3) modelling with fully coupled THM simulations Tier (4) to develop a look up function for dynamic stress conditions is new. Static stress can be mapped to dynamic stress conditions using a relatively simple formula, and so the stability under dynamic stress conditions can be expected to behave similarly to the stability under static conditions. The heterogeneity expected within the profile and the impact of thermal stress is then taken into account by comparing the numerical solution results with the Tier (3) results and augmenting the Tier (3) results with a factor to account for the dynamic stress conditions and heterogeneity.

Like any other geomechanical analysis the methodology requires that the stress profile is well known. The analytical solution in Tier (2) if it is only depth dependent assumes lateral stress consistency, and no significant changes due to thermal stress. Where this is not the case then the stability estimation will be inaccurate. However the better a regional profile is known the more accurate the predictions will be. In the case concerned it was clear that regionally the stress profile suggested an increase in gradient around about the commencement of the chalk group. An improvement on the analytical function could be the inclusion of the discrete depth of the chalk group. Extending this to other situation means that a good understanding of the stress profile as a function of the geomechanical facies could improve the accuracy of the results.

The empirical fitting of the analytical function is a further source of uncertainty. Empirical functions will tend to provide better fits in some areas of the data set than in other areas. Care needs to be taken that the depths represented within the storage complex are fitted adequately.

During the dynamic modelling, the larger scale heterogeneities can be taken into account, however although the grid scale can be of the order of 10 m or less, the data is provided typically with a horizontal accuracy at the best of 250 m and a vertical accuracy of the order of 1 m in the boreholes. Statistical interpretation can be used to "fill in the gaps", however they remain approximations of the system, and the results cannot be considered as a unique solution. This suggests caution in over stating the accuracy of the modelling results, and introduces realism into the accuracy of possible numerical simulations. In addition the parametrization of such large multi process models relies on laboratory, field and at time literature values, all of which carry differing degrees of uncertainty.

Taking into account the possible inaccuracies within the modelling approach, the predictions of the combinations of the modelling approaches (Tier 3 with a dynamic stress correction vs THM numerical model) are shown to be remarkably similar for two different sites, with different geometry and operational conditions. Therefore this methodology enabling the application of an empirical function based on an analytical evaluation of the static stress profile and a correction to account for the dynamic stress conditions and heterogeneity can be seen to provide a reasonable estimate of the geomechanical stability of the storage strata.

Further work could include the simulation of several further sections in the storage complex depending on the data available, in an attempt to improve the validity of the of the approach for deeper and shallower systems.

Summary of key modelling results

The following points provide a summary of the key findings of the modelling work

- The underburden contributes to the amount of pore space available to dissipate the increased pressure due to CO_2 injected into the reservoir
- The characteristics of the basal flow boundary and the nature of the Underburden have a very

significant impact on the regional development of a pressure signal due to CO_2 injection, and on the pressure connectivity of multiple sites

- The stability of the strata is related to the local stress field. The local stress field is dependent upon stress bridging effects caused by the material properties of the various strata. In the Captain Sandstone Fairway the depth of the Cretaceous Chalk defines a change in the rate of increase in the horizontal stress profile.
- Redistribution of regional stress due to overprint of thermal stress may in some situations increase the stability of the storage complex.
- As deeper reservoirs can maintain higher overpressures than shallow reservoirs, care needs to be taken in designing a multi-user store that the overall pressure signal does not compromise the safety of shallower areas of the reservoir due to pressure migration from the from deeper areas of the formation.
- The results of the analytical static stress modelling approach and the numerical dynamic stress modelling approach presented using an empirical function providing regional coverage of the storage asset and including implicitly all the complexity of the numerical heterogeneous calculations.

Conclusions

There will be an increased drive for the creation of large shared regional multi-user CO_2 storage assets in the near future as a technology to reduce CO_2 emissions to the atmosphere. Screening of complex stratigraphic stores will be necessary to predict and assess the integrity of existing and planned storage operations. One of the key factors which determine the integrity of a multi-user store is its geomechanical stability. The cumulative result of multiple CO_2 injection sites is that fluid pressure from different locations will be superimposed on one another.

Using a geomechanical facies approach, this paper has shown how analytical geomechanical models, empirical assumptions and numerical models can be combined to provide a simple but powerful tool for the prediction of the maximum overpressure possible in various strata, within fault systems and with a thermal stress overprint.

In addition the numerical modelling of the Captain Sandstone Fairway has highlighted the importance of including the Underburden in the fluid pressure calculations, both in terms of the nature of the basal boundary to flow, in providing access to additional pore space for storage, and as a major control in the regional pressure connectivity between injection sites.

The change in the stress field as a result of superposition of pore pressure within the reservoir and the thermal stress is dependent on the heterogeneity of the strata present. The distribution of fluid flow is dominated by the heterogeneity in permeability of different layers, which can easily be several orders of magnitude in difference. The mechanical parameters exhibit one or two orders of magnitude difference, where as the thermal parameters are all of the same magnitude. The thermal plume after injection for circa 30 years does not extend significantly beyond 500 metres from the injecting well, where as the fluid pressure field extends over several tens of kilometres. The nature of the strata overlying the injection point and underlying the injection well determines the response of the system to the combination of thermal stress and fluid pressure. Stress bridging can, in some cases, lead to enhanced stability in sealing rock layers as this redistributes the horizontal stress.

In a regionally extensive reservoir, as deeper parts of the reservoir can maintain higher overpressure values than shallower parts, care needs to be taken to design and manage a multi-user store so that the overall pressure signal does not compromise the integrity of a shallower store due to pressure migration from the from deeper strata. This leads to an interesting challenge to manage and optimise the time dependent pressure footprint of different injection sites.

The results of the analytical static stress modelling approach and the numerical dynamic stress modelling approach presented using an empirical function providing regional coverage of the storage asset and included implicitly all the complexity of the numerical heterogeneous calculations. This methodology significantly simplifies the evaluation of the geomechanical stability of extensive regional CO_2 storage assets.

Acknowledgements

The research leading to these results was conducted within the context of the CO2MultiStore project supported by and published with the permission of the Scottish Government, The Crown Estate, Scottish Enterprise, Shell and Vattenfall. It was also conducted within the context of the European Community's Seventh framework Programme FP7/2007-2013 under the grant agreement No. 282900 as part of the PANACEA project.

References

CAPPA, F., AND RUTQVIST, J., 2011, Modeling of coupled deformation and permeability evolution during fault reactivation induced by deep underground injection of CO2: International Journal of Greenhouse Gas Control, v. 5, p. 336-346.

CHANG, C., ZOBACK, M.D., AND KHAKSAR, A., 2006, Empirical relations between rock strength and physical properties in sedimentary rocks: Journal of Petroleum Science and Engineering, v. 51, p. 223-237.

DECC, 2013. Preferred bidders announced in UK's £1bn CCS Competition. Press release 13/028, 20 March 2013, UK Department of Energy & Climate Change Available at: https://www.gov.uk/government/news/preferred-bidders-announced-in-uk-s-1bn-ccs-competition

DE MARSILY, G. D., 1986, Quantitative hydrogeology : groundwater hydrology for engineers / Ghislain de Marsily; translated by Gunilla de Marsily, San Diego, Calif. ; London : Academic Press

EDLMANN, K., EDWARDS, M.A., QIAO, X.J., HASZELDINE, R.S., AND MCDERMOTT, C.I., 2014, Appraisal of global CO2 storage opportunities using the geomechanical facies approach: Environmental Earth Sciences, p. 1-22.

EU, 2011. Implementation of Directive 2009/31/EC on the geological storage of carbon dioxide – Guidance Document 2 – Characterisation of the storage complex, CO2 stream composition, monitoring and corrective measures.

FJAER, E., HOLT, R.M., HORSRUD, P., RAAEN, A. M. AND RISNES, R. 2008. Petroleum related rock mechanics, Second Edition, Hungary: Elsvier Science Ltd. ISBN 978-0-444-50260-5, p491

GEUZAINE, C., AND REMACLE, J.-F., 2009, Gmsh: A 3-D finite element mesh generator with built-in pre- and post-processing facilities: International Journal for Numerical Methods in Engineering, v. 79, p. 1309-1331.

HILLIS, R.R., 2001, Coupled changes in pore pressure and stress in oil fields and sedimentary basins: Petroleum Geoscience, v. 7, p. 419-425.

JAEGER, J., COOK, N., AND ZIMMERMAN, R., 2007, Fundamentals of rock mechanics 4th edition, Malden, USA: Blackwell Publishing Ltd.

JOHNSON, H., AND LOTT, G. K., 1993, 2. Cretaceous of the Central and Northern North Sea. in Lithostratigraphic nomenclature of the UK North Sea. KNOX, R W O'B. and CORDEY, W G. (editors). British Geological Survey, Nottingham.

KIM, S., AND HOSSEINI, S.A., 2014, Geological CO2 storage: Incorporation of pore-pressure/stress coupling and thermal effects to determine maximum sustainable pressure limit: Energy Procedia, v. 63, p. 3339-3346.

KNOX, R. W. O'B., AND HOLLOWAY, S., 1992, 1. Paleogene of the Central and Northern North Sea. in Lithostratigraphic nomenclature of the UK North Sea. KNOX, R W O'B. and CORDEY, W G. (editors). British Geological Survey, Nottingham.

KOLDITZ, O., BAUER, S., BILKE, L., BÖTTCHER, N., DELFS, J.O., FISCHER, T., GÖRKE, U.J., KALBACHER, T., KOSAKOWSKI, G., MCDERMOTT, C.I., PARK, C.H., RADU, F., RINK, K., SHAO, H., SHAO, H.B., SUN, F., SUN, Y.Y., SINGH, A.K., TARON, J., WALTHER, M., WANG, W., WATANABE, N., WU, Y., XIE, M., XU, W., AND ZEHNER, B., 2012, OpenGeoSys: An open-source initiative for numerical simulation of

thermo-hydro-mechanical/chemical (THM/C) processes in porous media: Environmental Earth Sciences, v. 67, p. 589-599.

KOLDITZ, O., GÖRKE, U.-J., SHAO, H., AND WANG, W., 2012, Thermo-hydro-mechanical-chemical processes in porous media: benchmarks and examples, Springer Science & Business Media, ISBN 978-3-642-27176-2, pp 391

LEWIS, R.W., AND SCHREFLER, B.A., 1998, The Finite Element Method in the Static and Dynamic Deformation and Consolidation of Porous Media: Chichester, England, John Wiley & Sons, 492 p.

MAGRI, F., TILLNER, E., WANG, W., WATANABE, N., ZIMMERMANN, G., AND KEMPKA, T., 2013, 3D Hydro-mechanical Scenario Analysis to Evaluate Changes of the Recent Stress Field as a Result of Geological CO2 Storage: Energy Procedia, v. 40, p. 375-383.

MCDERMOTT, C.I., LODEMANN, M., GHERGUT, I., TENZER, H., SAUTER, M., AND KOLDITZ, O., 2006a, Investigation of coupled hydraulic-geomechanical processes at the KTB site: Pressure-dependent characteristics of a long-term pump test and elastic interpretation using a geomechanical facies model: Geofluids, v. 6, p. 67-81.

MCDERMOTT, C.I., RANDRIAMANJATOSOA, A.R.L., TENZER, H., AND KOLDITZ, O., 2006b, Simulation of heat extraction from crystalline rocks: The influence of coupled processes on differential reservoir cooling: Geothermics, v. 35, p. 321-344.

PINNOCK, S.J., CLITHEROE, A.R.J., AND ROSE, P.T.S., 2003, The Captian Field, Block 13/22a, UK North Sea, *in* Gluyas, J.G.H., H.M., ed., United Kingdom Oil and Gas Fields, Commemorative Millennium Volume, Geological Society, London, Memoir, p. 431-441.

RUTQVIST, J., BIRKHOLZER, J., CAPPA, F., AND TSANG, C.F., 2006, Estimating maximum sustainable injection pressure during geological sequestration of CO2 using coupled fluid flow and geomechanical fault-slip analysis.

RUTQVIST, J., WU, Y.S., TSANG, C.F., AND BODVARSSON, G., 2002, A modeling approach for analysis of coupled multiphase fluid flow, heat transfer, and deformation in fractured porous rock: International Journal of Rock Mechanics and Mining Sciences, v. 39, p. 429-442.

SCCS, 2011. Progressing Scotland's CO2 Storage opportunities, 60pp. Available at: http://www.sccs.org.uk/images/expertise/reports/progressing-scotlands-co2/ProgressingScotlandCO2Opps.pdf

SCCS, 2015. Optimising CO2 storage in geological formations; a case study offshore Scotland, CO2MultiStore project. Scottish Centre for Carbon Storage Report, 76pp. ISBN: 978-085272-852-9 Available at: http://www.sccs.org.uk/images/expertise/reports/

SHELL 2011A. GEOMECHANICS SUMMARY REPORT. SCOTTISHPOWER CCS CONSORTIUM, UK CARBON CAPTURE AND STORAGE COMPETITION REPORT , UK CCS-KT-S7.19-SHELL-004, P.104

SHELL 2011B. PORE PRESSURE PREDICTION. SCOTTISHPOWER CCS CONSORTIUM, UK CARBON CAPTURE AND STORAGE COMPETITION REPORT , UK CCS-KT-S7.21-SHELL-006, P.30

SHELL 2011C. STATIC MODEL (AQUIFER). SCOTTISHPOWER CCS CONSORTIUM, UK CARBON CAPTURE AND STORAGE COMPETITION REPORT , UK CCS-KT-S7.22-SHELL-001, P.37

TENZER, H., PARK, C.H., KOLDITZ, O., AND MCDERMOTT, C.I., 2010, Application of the geomechanical facies approach and comparison of exploration and evaluation methods used at Soultz-sous-Forêts (France) and Spa Urach (Germany) geothermal sites: Environmental Earth Sciences, v. 61, p. 853-880.

VIDAL-GILBERT, S., NAUROY, J.-F., AND BROSSE, E., 2009, 3D geomechanical modelling for CO2 geologic storage in the Dogger carbonates of the Paris Basin: International Journal of Greenhouse Gas Control, v. 3, p. 288-299.

WILLIAMS, J., KIRK, K., AND MONAGHAN, A., 2013, Task 2.1 CO2MultiStore - Static geological model of the Captain Sandstone, risk reduction and knowledge exchange., British Geological Survey Internal Report., p. 61pp.

ZIENKIEWICZ, O.C., AND TAYLOR, R.L., 2005, The Finite Element Method, v. 1, Butterworth Heinemann, 752 p.

535